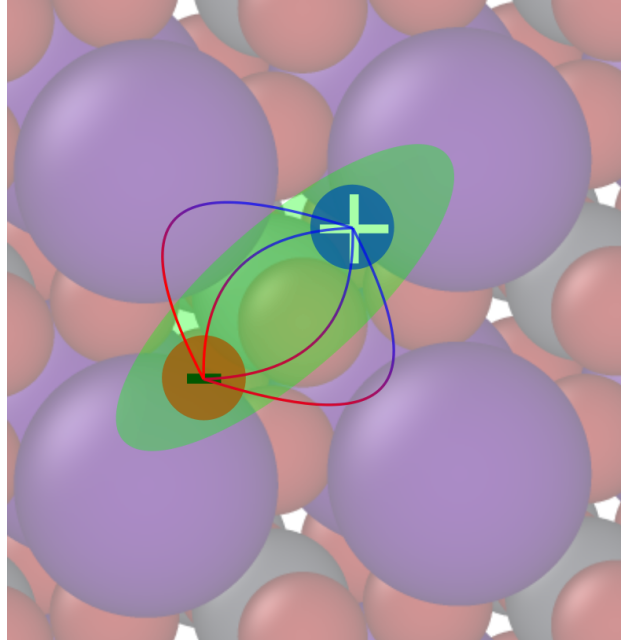
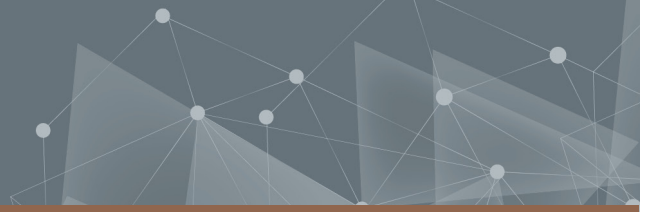




CHALMERS
UNIVERSITY OF TECHNOLOGY



Excitons in Perovskites

Microscopic Modelling of Exciton Spectra in Perovskites and Exciton-Phonon Coupling

Master's thesis in Physics

AMBJÖRN JOKI

DEPARTMENT OF PHYSICS
CHALMERS UNIVERSITY OF TECHNOLOGY
Gothenburg, Sweden 2022
www.chalmers.se

MASTER'S THESIS 2022

Excitons in Perovskites

Microscopic Modelling of Exciton Spectra in Perovskites and
Exciton-Phonon Coupling

AMBJÖRN JOKI



CHALMERS
UNIVERSITY OF TECHNOLOGY

Department of Physics
Division of Condensed Matter and Materials Theory
Computational Materials Group
CHALMERS UNIVERSITY OF TECHNOLOGY
Gothenburg, Sweden 2022

Excitons in Perovskites
Microscopic Modelling of Exciton Spectra in Perovskites and Exciton-Phonon Coupling
AMBJÖRN JOKI

© AMBJÖRN JOKI, 2022.

Supervisors: Raül Perea Causín and Ermin Malic, Department of Physics
Examiner: Paul Erhart, Department of Physics Department

Master's Thesis 2022
Department of Physics
Division of Condensed Matter and Materials Theory
Computational Materials Group
Chalmers University of Technology
SE-412 96 Gothenburg
Telephone +46 31 772 1000

Cover: An exciton in a general cubic 3D perovskite.

Typeset in L^AT_EX
Printed by Chalmers Reproservice
Gothenburg, Sweden 2022

Excitons in Perovskites
Microscopic Modelling of Exciton Spectra in Perovskites and Exciton-Phonon Coupling
Ambjörn Joki
Department of Physics
Chalmers University of Technology

Abstract

Perovskites are interesting materials due to their special optoelectronic properties — properties already being used in photovoltaics and potentially in future light-emitters. Since perovskites exhibit strongly bound excitons, the excitons are, often still at room temperature, crucial to consider. In this work a model aimed at describing the excitonic landscape in 2D and 3D perovskites has been developed. The model includes the exchange interaction giving rise to an exciton fine structure consisting of optically active and inactive exciton states, the latter with lower energy. The model is further extended by inclusion of a magnetic field, necessary in experimental setups to probe the inactive states. The developed model captures the qualitative excitonic aspects of 3D perovskites predicting three optically active states and one inactive, but is incomplete in the 2D case predicting two active and two inactive states. The incompleteness is probably related to the treatment of the confined direction in 2D. Further, the exciton phonon scattering between active and inactive states is modelled. For applications the phonon scattering is important since high scattering rates will transfer many excitons from optically active states to the inactive one with lower energy, reducing the light emission. However, indications of a phonon bottleneck — reduced scattering rate — have been observed. Assuming spin conservation, the phonon scattering between active and non-active states is found to be non-existing — thus further confirming the phonon bottleneck. The model contributes to better microscopic understanding of the exciton-phonon coupling in perovskites.

Keywords: bright excitons, dark excitons, phonon-exciton scattering, phonon-bottlenecks, perovskites, magnetic field

Acknowledgements

Firstly, I would like to thank my supervisor Raül for introducing me to this field and enduring my endless questions. I would also like to thank my supervisor Ermin and supervisor and examiner Paul for making this project possible.

Ambjörn Joki, Gothenburg, June 2022

List of Acronyms

Below is the list of acronyms that have been used throughout this thesis listed in alphabetical order:

COM	Center of mass momentum
PEA	Polyethylene adipate
SOC	Spin orbit coupling

Contents

List of Acronyms	ix
List of Figures	xiii
List of Tables	xv
1 Introduction	1
2 Theory	3
2.1 Excitons	3
2.2 Coupling	5
3 Perovskites	9
4 Exciton Landscape	13
4.1 Inclusion of Exchange Interaction	13
4.2 Perturbation	16
4.3 Effect of Spin Orbit Coupling	17
4.4 Exciton States	18
4.4.1 Characterization of States	20
4.5 Landscape in 2D	21
4.6 Value of Bright-Dark Energy Splitting	22
4.6.1 3D	22
4.6.2 2D	22
5 Magnetic Field	25
6 Phonon Scattering	29
6.1 Scattering With Spin Conservation	29
6.2 Scattering Without Spin Conservation	30
7 Discussion	31
Bibliography	35
A Perturbation	I
B Vector Components of Dipole Matrix Elements	VII

List of Figures

3.1	The standard cubic perovskite structure, note that there are a lot of different varieties of this structure still considered to be perovskites. Reproduced with permission [1].	9
3.2	Bandstructure of PEA_2PbI_4 when approximated as cubic, note the bandgap at the Γ -point and no dispersion in the z-direction, Γ to Z.	10
4.1	The figure shows the band structure around the band gap for the conduction and valence band in a parabolic approximation. Momentum on the x -axis and energy on the y -axis. Electrons are denoted by red circles. Black arrows indicate momentum change of electrons within bands and green the equivalent exchange process.	14
4.2	Total energy and short and long range energies for PEA_2PbI_4	23
5.1	Values of coefficients in 3D. Note that Ψ_L^- has the highest absolute valued dark state coefficient. The g -factors of PEA_2PbI_4 have been used since ultimately measurements on that perovskite is the ones compared with. The T^+ and T^- coefficients are overlapping.	27
5.2	Energy levels in 2D and 3D. The magnetic field results in four non-degenerate energies. The g -factors of PEA_2PbI_4 have been used in both cases.	27
7.1	The figures shows the band structure around the gamma point for conduction and valence band under parabolic approximation. Momentum on the x -axis and energy on the y -axis. Electrons are denoted by red circles and phonons with a red arrow. Black arrows indicates momentum change of electrons within bands and green the equivalent exchange process. The latter allowing for a spin change.	34

List of Tables

3.1	Material constants of PEA_2PbI_4	11
3.2	Material constants of studied 3D perovskites [2].	11
4.1	Bright-dark energy splitting for three cubic 3D perovskites according to Eq. (4.31).	22
6.1	Values of the transition constant C between 1s states with no magnetic field but with spin flip allowed.	30

1

Introduction

Perovskites are interesting materials due to their special optoelectronic properties [3] — properties that are useful for solar cell applications and potentially in future light-emitters. These properties are influenced by excitons [4] which in both 2D and 3D perovskites are relatively strongly bound, with binding energies up to hundreds of meV [3, 4]. Microscopic understanding of the excitons makes prediction of material properties more precise and due to the extensive tunability of perovskites, offers a plethora of options for synthesizing materials with desired properties.

For applications within light emission, the exciton fine structure of perovskites is important. The fine structure, arising from the spin degeneracy of the conduction and valance bands together with the exchange interaction, comprises both optically active (bright) and optically inactive (dark) states [2, 5]. The dark states could reduce the emission efficiency considerably, especially if the lowest energy state is dark, since in thermal equilibrium a high population of that state would be expected. Apart from the energetic ordering of the states, the scattering channels between them are also crucial. If the bright states cannot scatter down to lower dark states efficiently, the emission loss decreases.

In a recent experimental paper [5], the fine structure of the optical emission of three 2D perovskites was studied. Applying a magnetic field, the lowest dark state was brightened and found to have lower energy than the lowest bright states. Furthermore, the occupation of the states was found to not follow a thermal distribution possibly due to a so called phonon bottleneck. The bottleneck indicates inefficient scattering between the bright states, where the excitons end up after optical excitation, and the dark state.

The aim of this project is to develop a model based on second quantization to describe the exciton spectrum both qualitatively and quantitatively. Of special interest is the ordering of states and energy difference between the bright and dark states, since the relationship between the bright-dark energy splitting and the energy of available phonons, is believed to directly affect phonon scattering. The final aim is to model the phonon scattering and find possible explanations for its predicted inefficiency.

The report is divided into three parts. In the first the theory required for the project is discussed together with some important aspects of the studied material system. In the second, the model of the exciton spectrum is developed with and without magnetic field. This part finishes with a short evaluation of single electron phonon scattering with and without spin conservation. In the final part and chapter, the quality of the developed model, especially the treatment of the 2D perovskites, is discussed. The phonon scattering is also addressed.

2

Theory

It is often convenient to use the formalism of second quantization within many body physics. Fundamental for second quantization are the creation and annihilation of particles, described by operators $a^{(\dagger)}$. Important properties of these operators are their commutators

$$\begin{aligned} [a_i^{(\dagger)}, a_j^{(\dagger)}]_{\pm} &= a_i^{(\dagger)} a_j^{(\dagger)} \pm a_j^{(\dagger)} a_i^{(\dagger)} = 0 \\ [a_i, a_j^{\dagger}]_{\pm} &= \delta_{i,j} \end{aligned} \quad (2.1)$$

where the minus and plus signs apply for bosons and fermions, respectively. These relations make the wavefunctions created using the annihilation and creation operators automatically symmetric or anti-symmetric as applicable. Using the operators it is possible to describe different states and interactions. Based on the formalism it is possible to show how excitons arise conceptually. Furthermore, by regarding the coupling of electrons to their surroundings, it becomes possible to also describe the coupling of excitons.

2.1 Excitons

Excitons may be viewed as hydrogenic systems consisting of a positive and a negative charge. For the excitons these are not a nucleus and an electron but rather a hole and an electron. The oppositely charged particles attract each other reducing the energy of the system. The exciton states and binding energies can be compared with and are named in equivalence to the orbital states of a hydrogen atom. The symmetry of the wavefunctions corresponds to the respective orbital wavefunctions. The energy of an exciton may be considered to be the energy of the electron, the hole as well as the Coulomb interaction between these. In second quantization in a two-band model the Hamiltonian is

$$H = \sum_{\mathbf{k},s} E_{\mathbf{k}}^c c_{\mathbf{k}s}^{\dagger} c_{\mathbf{k}s} - \sum_{\mathbf{k}',s} E_{\mathbf{k}'}^v v_{\mathbf{k}'s} v_{\mathbf{k}'s}^{\dagger} - \sum_{\substack{\mathbf{k},\mathbf{k}' \\ s,s' \\ \mathbf{q}}} c_{\mathbf{k}'+\mathbf{q},s}^{\dagger} v_{\mathbf{k},s'} v_{\mathbf{k}-\mathbf{q},s'}^{\dagger} c_{\mathbf{k}',s} V_{v,\mathbf{k},s';c,\mathbf{k}',s}^{c,\mathbf{k}'+\mathbf{q},s;v,\mathbf{k}-\mathbf{q},s'}. \quad (2.2)$$

Here, $E_{\mathbf{k}}^c$ is the energy of an electron in the conduction band, $E_{\mathbf{k}}^v$ is the energy of an electron in the valance band and the third term describes the contribution from a momentum transfer \mathbf{q} between two electrons in different bands — the Coulomb interaction. The attractive Coulomb force reduces the energy of the exciton which therefore is smaller than the band gap $E_g = E^c - E^v$.

As an exciton is a bound electron-hole pair, it is sometimes better to view it as a quasi-particle rather than two separate (quasi-)particles. The first step of rewriting the Hamiltonian in an exciton basis may be taken by introducing pair operators (P), defining the creation and annihilation of an exciton

$$\begin{aligned} c_{\mathbf{k}s}^\dagger v_{\mathbf{k}'s'} &= P_{\mathbf{k}s\mathbf{k}'s'}^\dagger \\ v_{\mathbf{k}'s'}^\dagger c_{\mathbf{k}s} &= P_{\mathbf{k}s\mathbf{k}'s'}, \end{aligned} \quad (2.3)$$

where $P_{\mathbf{k}s\mathbf{k}'s'}^{(\dagger)}$ implies annihilation (creation) of an electron with momentum \mathbf{k} and spin s in the conduction band and creation (annihilation) of one electron with momentum \mathbf{k}' and spin s' in the valance band.

The first and second term of Eq. (2.2) do not represent exciton annihilation or creation. When expressing these in the pair-operator picture, approximations are required [6, 7]

$$\begin{aligned} c_{\mathbf{k}s}^\dagger c_{\mathbf{k}s} &\approx \sum_{\mathbf{k}',s'} P_{\mathbf{k}s\mathbf{k}'s'}^\dagger P_{\mathbf{k}s\mathbf{k}'s'} - \frac{1}{2} \sum_{\substack{\mathbf{k}',\mathbf{k}_1,\mathbf{k}_2 \\ s',s_1,s_2}} P_{\mathbf{k}s\mathbf{k}'s'}^\dagger P_{\mathbf{k}_1s_1\mathbf{k}_2s_2}^\dagger P_{\mathbf{k}_1s_1\mathbf{k}_2s_2} P_{\mathbf{k}s\mathbf{k}'s'} \\ v_{\mathbf{k}s} v_{\mathbf{k}s}^\dagger &\approx \sum_{\mathbf{k}',s'} P_{\mathbf{k}'s'\mathbf{k}s}^\dagger P_{\mathbf{k}'s'\mathbf{k}s} - \frac{1}{2} \sum_{\substack{\mathbf{k}',\mathbf{k}_1,\mathbf{k}_2 \\ s',s_1,s_2}} P_{\mathbf{k}'s'\mathbf{k}s}^\dagger P_{\mathbf{k}_1s_1\mathbf{k}_2s_2}^\dagger P_{\mathbf{k}_1s_1\mathbf{k}_2s_2} P_{\mathbf{k}'s'\mathbf{k}s} \end{aligned}$$

for equality an infinite number of pair-operator terms needs to be included. Since it is often possible to assume low excitation densities, only including the first term, however, often yields a fair approximation.

The final step is to change into an exciton basis, described by exciton annihilation and creation operators $X_{\mathbf{Q}}^{\nu s s'(\dagger)}$ where ν is the state of the exciton, \mathbf{Q} the center of mass momentum (COM) defined as $\mathbf{k} - \mathbf{k}' = \mathbf{Q}$ and s (s') is the spin of the electron (vacant electron state). Note that the spins are defined in the electron-electron picture, the spin of the hole is related to the spin of the empty electron state via the time reversal operator \hat{K} as $\hat{K}s = \sigma_s \bar{s}$ where \bar{s} denotes the opposite spin of s and σ_s is 1 for spin up and -1 for spin down [2]. Further the relative momentum is defined as $\tilde{\mathbf{k}} = \alpha_h \mathbf{k}_e + \alpha_e \mathbf{k}_h$ with $\alpha_i = \frac{m_i}{m_e + m_h} = \frac{m_i}{M}$ where e (h) stands for electron (hole). Then the pair-operator and exciton pictures are related according to

$$\begin{aligned} c_{\mathbf{k}s}^\dagger v_{\mathbf{k}'s'} &= P_{\mathbf{k}s\mathbf{k}'s'}^\dagger = \sum_{\nu} \phi_{\alpha_h \mathbf{k} + \alpha_e \mathbf{k}'}^{\nu} X_{\mathbf{k}-\mathbf{k}'}^{\nu s s' \dagger} \\ v_{\mathbf{k}'s'}^\dagger c_{\mathbf{k}s} &= P_{\mathbf{k}s\mathbf{k}'s'} = \sum_{\mu} \phi_{\alpha_h \mathbf{k} + \alpha_e \mathbf{k}'}^{\mu*} X_{\mathbf{k}-\mathbf{k}'}^{\mu s s'} \\ c_{\mathbf{k}s}^\dagger c_{\mathbf{k}s} &= \sum_{\mathbf{k}',s'} P_{\mathbf{k}s\mathbf{k}'s'}^\dagger P_{\mathbf{k}s\mathbf{k}'s'} = \sum_{\mathbf{k}',s',\nu,\mu} \phi_{\alpha_h \mathbf{k} + \alpha_e \mathbf{k}'}^{\nu} X_{\mathbf{k}-\mathbf{k}'}^{\nu s s' \dagger} \phi_{\alpha_h \mathbf{k} + \alpha_e \mathbf{k}'}^{\mu*} X_{\mathbf{k}-\mathbf{k}'}^{\mu s s'} \\ v_{\mathbf{k}s} v_{\mathbf{k}s}^\dagger &= \sum_{\mathbf{k}'',s''} P_{\mathbf{k}''s''\mathbf{k}s}^\dagger P_{\mathbf{k}''s''\mathbf{k}s} = \sum_{\mathbf{k}'',s'',\nu,\mu} \phi_{\alpha_h \mathbf{k}'' + \alpha_e \mathbf{k}}^{\nu} X_{\mathbf{k}''-\mathbf{k}}^{\nu s'' s \dagger} \phi_{\alpha_h \mathbf{k}'' + \alpha_e \mathbf{k}}^{\mu*} X_{\mathbf{k}''-\mathbf{k}}^{\mu s'' s} \end{aligned} \quad (2.4)$$

Using the relations in Eqs. (2.4) the Hamiltonian in Eq. (2.2) may be expressed as

$$\begin{aligned}
 H = & \sum_{s,\mathbf{k}} E_{\mathbf{k}}^c \sum_{\mathbf{k}',s',\nu,\mu} \phi_{\alpha_h \mathbf{k} + \alpha_e \mathbf{k}'}^\nu X_{\mathbf{k}-\mathbf{k}'}^{\nu s s' \dagger} \phi_{\alpha_h \mathbf{k} + \alpha_e \mathbf{k}'}^{\mu*} X_{\mathbf{k}-\mathbf{k}'}^{\mu s s'} \\
 & - \sum_{s,\mathbf{k}'} E_{\mathbf{k}'}^v \sum_{\mathbf{k}'',s'',\nu,\mu} \phi_{\alpha_h \mathbf{k}'' + \alpha_e \mathbf{k}'}^\nu X_{\mathbf{k}''-\mathbf{k}'}^{\nu s'' s' \dagger} \phi_{\alpha_h \mathbf{k}'' + \alpha_e \mathbf{k}'}^{\mu*} X_{\mathbf{k}''-\mathbf{k}'}^{\mu s'' s} \\
 & - \sum_{\substack{\mathbf{k},\mathbf{k}' \\ s,s'}} \sum_{\nu} \phi_{\alpha_h (\mathbf{k}'+\mathbf{q}) + \alpha_e \mathbf{k}}^\nu X_{\mathbf{k}'+\mathbf{q}-\mathbf{k}}^{\nu s s' \dagger} \sum_{\mu} \phi_{\alpha_h \mathbf{k}' + \alpha_e (\mathbf{k}-\mathbf{q})}^{\mu*} X_{\mathbf{k}'-(\mathbf{k}-\mathbf{q})}^{\mu s s'} V_{\mathbf{q}},
 \end{aligned} \tag{2.5}$$

details on how the Coulomb term $V_{v,k,s';c,k',s}^{c,k'+q,s;v,k-q,s'}$ was expanded can be found in section 4.1. By noting that $\mathbf{k}_e = \mathbf{k} = \mathbf{k}''$ and $\mathbf{k}_h = \mathbf{k}'$ shifting $s \rightarrow s'$ and $s'' \rightarrow s$ in the second term and $\mathbf{k} \rightarrow \mathbf{k} + \mathbf{q}$ in the third, Eq. (2.5) may be rewritten as

$$\begin{aligned}
 H = & \sum_{\substack{\mathbf{Q},\hat{\mathbf{k}} \\ \nu,\mu,s,s'}} \phi_{\hat{\mathbf{k}}}^\nu \phi_{\hat{\mathbf{k}}}^{\mu*} X_{\mathbf{Q}}^{\nu s s' \dagger} X_{\mathbf{Q}}^{\mu s s'} (E_{\hat{\mathbf{k}} + \alpha_e \mathbf{Q}}^c - E_{\hat{\mathbf{k}} - \alpha_h \mathbf{Q}}^v) - \sum_{\substack{\mathbf{Q},\hat{\mathbf{k}} \\ \mu,\nu,s,s'}} \phi_{\hat{\mathbf{k}}+\mathbf{q}}^\nu X_{-\mathbf{Q}}^{\nu s s' \dagger} \phi_{\hat{\mathbf{k}}}^{\mu*} X_{-\mathbf{Q}}^{\mu s s'} V_{\mathbf{q}} \\
 = & \sum_{\substack{\mathbf{Q},\hat{\mathbf{k}} \\ \nu,\mu,s,s'}} \left((E_{\hat{\mathbf{k}} + \alpha_e \mathbf{Q}}^c - E_{\hat{\mathbf{k}} - \alpha_h \mathbf{Q}}^v) \phi_{\hat{\mathbf{k}}}^\nu - \sum_{\mathbf{q}} \phi_{\hat{\mathbf{k}}+\mathbf{q}}^\nu V_{\mathbf{q}} \right) \phi_{\hat{\mathbf{k}}}^{\mu*} X_{\mathbf{Q}}^{\nu s s' \dagger} X_{\mathbf{Q}}^{\mu s s'} \\
 = & \sum_{\substack{\mathbf{Q},\hat{\mathbf{k}} \\ \nu,\mu,s,s'}} \left(\frac{\hbar^2 \mathbf{Q}^2}{2M} + \underbrace{\frac{\hbar^2 \hat{\mathbf{k}}^2}{2m_\mu} - \sum_{\mathbf{q}} \phi_{\hat{\mathbf{k}}+\mathbf{q}}^\nu V_{\mathbf{q}}}_{E^\nu \phi_{\hat{\mathbf{k}}}^\nu} \right) \phi_{\hat{\mathbf{k}}}^{\mu*} X_{\mathbf{Q}}^{\nu s s' \dagger} X_{\mathbf{Q}}^{\mu s s'} \\
 = & \sum_{\substack{\mathbf{Q} \\ \mu,s,s'}} \left(\frac{\hbar^2 \mathbf{Q}^2}{2M} + E^\nu \right) X_{\mathbf{Q}}^{\nu s s' \dagger} X_{\mathbf{Q}}^{\mu s s'}.
 \end{aligned} \tag{2.6}$$

Here, the electron energy around the band gap has been approximated as parabolic $E_{\hat{\mathbf{k}}}^\lambda = \sigma_\lambda \frac{\hbar^2 \hat{\mathbf{k}}^2}{2m_\lambda}$ with $\sigma_c = -\sigma_v = 1$, E^ν is the binding energy of the exciton in state ν and the relation $\sum_{\hat{\mathbf{k}}} \phi_{\hat{\mathbf{k}}}^\nu \phi_{\hat{\mathbf{k}}}^{\mu*} = \delta_{\mu,\nu}$ has been used. The result is the dispersion describing the energy of an exciton with COM \mathbf{Q} .

2.2 Coupling

One of the ways excitons may be created is by photon absorption, when an electron is moved to the conduction band leaving a hole in the valance band. Excitons that may be created by simply absorbing a photon are called bright excitons and excitons which require more complex processes are called dark. There are different reasons behind an exciton state being dark, one reason is momentum as in TMDs and carbon nanotubes [8, 9, 10] another is spin, which arises when the considered valance and conduction bands have different spin. For an electron-excitation an additional spin flip process is therefore required.

Mathematically the coupling between electrons and light is, treating light classically, described by

$$H_{el-li} = e_0 \sum_{i,j} \mathbf{A} \cdot \mathbf{d}^{ij} \lambda_i^\dagger \lambda_j \quad (2.7)$$

where \mathbf{A} is the electromagnetic vector potential, e_0 the electron charge and the optical matrix elements $\mathbf{d}^{i,j} = \langle i | \hat{\mathbf{p}} | j \rangle$ describes a transition from state j to i . The exciton is dark if the quantity $\mathbf{A} \cdot \mathbf{d}$ vanishes. In experimental setups, the vector field is sometimes lacking a component in some direction, say \hat{z} . In this case an exciton associated with a non-zero optical matrix element only in the z -direction $\mathbf{d}^{i,j} \propto \hat{z}$, would not couple to the field and effectively be dark. Such excitons can be referred to as gray.

Another important type of coupling is the one with phonons (collective motions of the nuclei in a crystal lattice [11]), known as phonon scattering. Phonons are usually divided into two groups: acoustic modes whose energy is proportional to their momentum and optical modes with in general higher energies. Due to the low velocities but heavy masses of nuclei, phonons carry in general relatively low energy but high momentum. The relatively high momentum of phonons opens up for new relaxation channels by allowing changes of the exciton COM. The scattering with phonons can both be within bands (intraband) and in between bands (interband). The general electron-phonon interaction in the electron picture can be expressed as

$$\sum_{s,s',\lambda,\mathbf{q},\mathbf{k},j} g_q^{j,\lambda} \lambda_{\mathbf{k}+\mathbf{q},s}^\dagger \lambda_{\mathbf{k},s'} b_q^j + g_q^{j,\lambda} \lambda_{\mathbf{k}-\mathbf{q},s}^\dagger \lambda_{\mathbf{k},s'} b_q^{j\dagger}, \quad (2.8)$$

where the first term describes the creation of an electron with momentum $\mathbf{k} + \mathbf{q}$ after annihilation of one electron with momentum \mathbf{k} and a phonon with momentum \mathbf{q} , in other words an electron taking up momentum \mathbf{q} from a phonon. In the same way the second term describes an electron creating a phonon losing a momentum \mathbf{q} . The coupling elements g in Eq. (2.8) is given by [12]

$$H_{ex-ph} = g_q^{j,\lambda} = D_q^{j,\lambda} \sqrt{\frac{\hbar^2}{2\rho\hbar\omega_q^j}}, \quad (2.9)$$

where the deformation potential $D_q^{j,\lambda}$ is given by $D_q^{j,\lambda} = D_{\text{OP}}^{j,\lambda}$ for optical modes and $D_q^{j,\lambda} = qD_{\text{AC}}^{j,\lambda}$ for acoustic modes, $\hbar\omega_q^j$ is the energy of the phonon and ρ the density of the material.

If only considering one conduction and one valance band $\lambda = \{c, v\}$, summing over λ and using the relations in Eq. (2.4) to rewrite in exciton picture, the following exciton-phonon coupling expression is obtained

$$H_{ex-ph} = \sum_{\substack{s,s',s'' \\ \mathbf{q},\mathbf{Q},\tilde{\mathbf{k}} \\ j,\nu,\mu}} g_q^{j,c} \phi_{\tilde{\mathbf{k}}+\alpha_h\mathbf{q}}^\nu \phi_{\tilde{\mathbf{k}}}^{\mu*} X_{\mathbf{Q}+\mathbf{q}}^{\nu s s''\dagger} X_{\mathbf{Q}}^{\mu s' s''} b_q - g_q^{j,v} \phi_{\tilde{\mathbf{k}}-\alpha_e\mathbf{q}}^\nu \phi_{\tilde{\mathbf{k}}}^{\mu*} X_{\mathbf{Q}+\mathbf{q}}^{\nu s'' s'\dagger} X_{\mathbf{Q}}^{\mu s'' s} b_q + H.C. \quad (2.10)$$

where H.C. stands for the Hermitian conjugate of the two first terms. If $s = s' = s''$ and spin degeneracy is neglected, the expression can be rewritten

$$H_{ex-ph} = \sum_{\substack{\mathbf{q},\mathbf{Q},\tilde{\mathbf{k}} \\ j,\nu,\mu}} G_q^{\nu\mu j*} X_{\mathbf{Q}+\mathbf{q}}^{\nu\dagger} X_{\mathbf{Q}}^\mu b_q + G_q^{\nu\mu j} X_{\mathbf{Q}}^{\mu\dagger} X_{\mathbf{Q}+\mathbf{q}}^\nu b_q^\dagger \quad (2.11)$$

with

$$G_{\mathbf{q}}^{\nu\mu j*} = \sum_{\mathbf{k}} \phi_{\mathbf{k}}^{\nu} (\phi_{\mathbf{k}+\alpha_h\mathbf{q}}^{\mu*} g_{\mathbf{q}}^{j,c} - \phi_{\mathbf{k}-\alpha_e\mathbf{q}}^{\mu*} g_{\mathbf{q}}^{j,v}) \quad (2.12)$$

where $\alpha_i = \frac{m_i}{\mu}$ and the wavefunctions represent the initial and final states [3]. Thus the overlap of the wavefunctions is important for the scattering strength, the strength is given by

$$\Gamma_{\mathbf{k}}^{\nu} = \pi \sum_{j,\mathbf{q},\pm,\mu} |G_{\mathbf{q}}^{\nu\mu j}|^2 \left(n_{\mathbf{q}}^j + \frac{1}{2} \pm \frac{1}{2} \right) \delta(E_{\mathbf{k}+\mathbf{q}}^{\mu} - E_{\mathbf{k}}^{\nu} \pm \hbar\Omega_{\mathbf{q}}^j) \quad (2.13)$$

where the sum is over all possible final exciton states μ , all phonon modes j and transferred momentum \mathbf{q} [3, 13]. The plus corresponds to emission and minus to absorption of a phonon and $n_{\mathbf{q}}^j$ is the number of phonons in the system.

A third possible interaction is that with a magnetic field. The Hamiltonian describing the energy of electrons in an in-plane magnetic field with strength B is given by

$$H_{el-mag} = \sum_{s,s',\lambda,\mathbf{k}} B \frac{g^{\lambda}}{2} \mu_B \lambda_{\mathbf{k},s}^{\dagger} \lambda_{\mathbf{k},s'}, \quad (2.14)$$

where g^{λ} is the magnetic coupling constant relevant for a magnetic field in-plane, which may be different between different bands, and $\mu_B = \frac{e\hbar}{2m}$ is the Bohr magneton [14]. Rewriting into an exciton basis the magnetic Hamiltonian is

$$H_{el-mag} = \sum_{\substack{\tilde{\mathbf{k}}, \mathbf{Q} \\ s_1, s_2, s_3, s_4 \\ \mu, \nu}} \frac{B\mu_B}{2} (g^c \delta_{s_2, s_4} \delta_{s_1, \bar{s}_3} - g^v \delta_{s_2, \bar{s}_4} \delta_{s_1, s_3}) \phi_{\tilde{\mathbf{k}}}^{\nu} \phi_{\tilde{\mathbf{k}}}^{\mu*} X_{\mathbf{Q}}^{\mu s_1 s_4 \dagger} X_{\mathbf{Q}}^{\mu s_3 s_2}. \quad (2.15)$$

Apart from shifting energies the magnetic field may also mix states, brightening spin-dark excitons [15].

3

Perovskites

Perovskite is the common name of materials having perovskite structure [1]. They share the chemical formula ABX_3 and a unit cell which is made up from B ions in the corners, an octahedron of X ions around each B ion, and an A ion at the center of the cell, see Figure 3.1. The A, B and X ions may be many different elements, resulting in many different materials with the perovskite structure [1]. In addition there are many structures apart from the cubic referred to as perovskites. Some perovskites exhibit strongly bound excitons and optical properties dependent on the excitons [4].

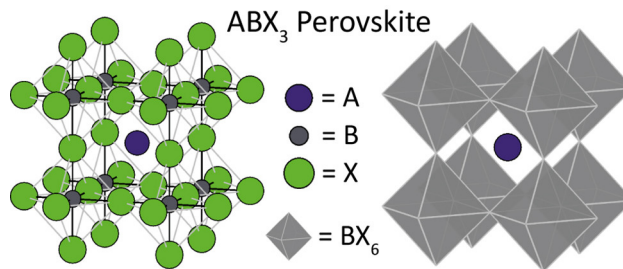


Figure 3.1: The standard cubic perovskite structure, note that there are a lot of different varieties of this structure still considered to be perovskites. Reproduced with permission [1].

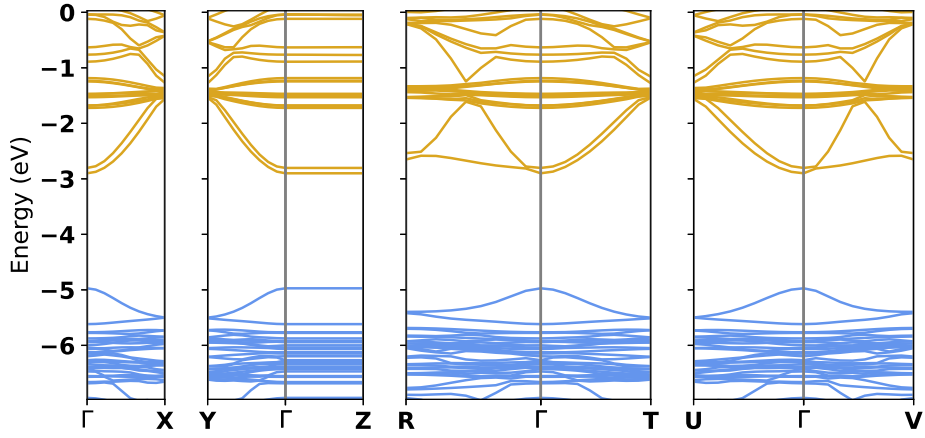
A special case of the perovskite structures are the two dimensional ones. In these all or a fraction of the A ions are replaced by large organic ions (L) resulting in a layered material [1]. These materials, described by the chemical formula $L_m A_{n-1} B_n X_{3n+1}$ where n is the number of inorganic layers connected to each other and m depends on n , are often called 2D perovskites, although they are strictly speaking not perovskites [1]. The alteration of inorganic and wide organic layers with different dielectric constants leads to the formation of effective quantum wells [1]. As in other 2D materials the reduced screening in one dimension leads to increased binding energies of the excitons. However, as a difference to, for example, graphene, 2D perovskites are not single layer materials but really a bulk material.

If the perovskites are approximated as cubic they exhibit one band gap at the Γ -point, see Figure 3.2 for the full band structure of PEA_2PbI_4 with and without spin orbit coupling (SOC). Note also that there is no band dispersion in the z -direction, from the Γ -point to the Z-point, indicating the confinement in the z -direction. In lead halide perovskites the conduction band is mainly formed by lead P -orbitals and the valance band mainly by halide S -orbitals. Without SOC the conduction band would

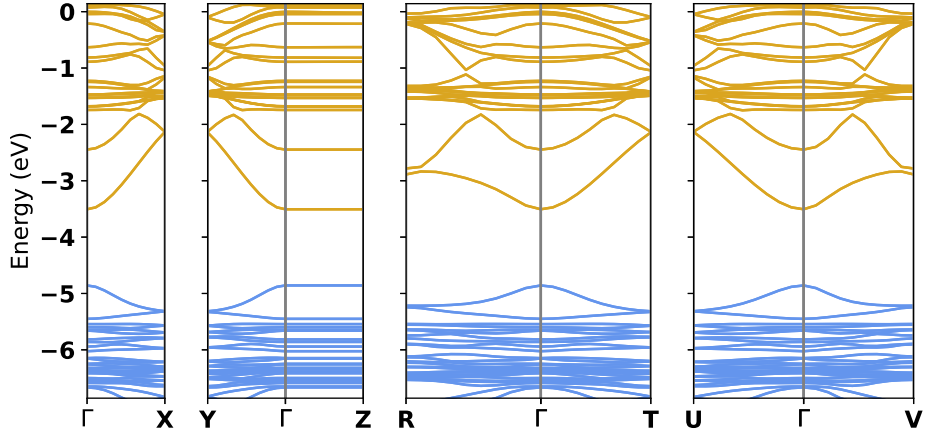
be sixfold degenerate, this degeneracy is however lifted when accounting for SOC. Including SOC the conduction band is split into a doubly degenerate lower band and a fourfold degenerate upper band. Furthermore the spins and orbital states are mixed so that the Bloch functions in the conduction band are not purely spin up or down, but are, in symmetries O_h , D_{4h} and D_{2h} , up to a phase factor given by [16]

$$|u_{cks}\rangle = |cs\rangle = (\alpha |P_x\bar{s}\rangle + i\beta\sigma_s |P_y\bar{s}\rangle + \gamma |P_zs\rangle), \quad (3.1)$$

where \bar{s} denotes the opposite spin of s . In a cubic symmetry the factors are $\alpha = \pm\beta = \pm\gamma = -\frac{1}{\sqrt{3}}$ [2] where the plus is chosen for spin up and minus for spin down.



(a) Without SOC.



(b) With SOC.

Figure 3.2: Bandstructure of PEA_2PbI_4 when approximated as cubic, note the bandgap at the Γ -point and no dispersion in the z -direction, Γ to Z .

Further, both 3D and 2D perovskites exhibit strongly bound excitons still forming at room temperature [4]. These excitons are important for the optical properties of the material. The dynamics of the excitons are governed by the scattering with phonons

and in perovskites particularly with optical phonons since the coupling to the acoustic modes is weak [3, 5]. Therefore, as the dynamics of the excitons is dependent on electron-phonon coupling, so are the optical properties of the perovskites [17].

The material constants of studied perovskites are presented in Tables 3.1 and 3.2. The constants are the width of the inorganic layer L_{well} , the dielectric constants of the inorganic layer and surrounding organic layers ϵ_{well} and ϵ_{org} , the effective mass of the electrons (holes) $m_{e(h)}$ given in electron masses, the band gap E_g and the effective g factors $g_T = g^c + g^v$ and $g_L = g^c - g^v$ as defined in [5].

Constant/Perovskite	PEA ₂ PbI ₄
L_{well} (nm)	0.636 [3]
ϵ_{well}	6.1 [3]
ϵ_{org}	3.32 [3]
m_e (m_0)	0.19 [18]
m_h (m_0)	0.25 [18]
E_g (eV)	2.565 [3]
g_T	4 ± 0.3 [5]
g_L	1.9 ± 0.5 [5]

Table 3.1: Material constants of PEA₂PbI₄.

Constant/Perovskite	CsPbCl ₃	CsPbBr ₃	CsPbI ₃
ϵ_{in}	4.5	4.8	5.0
m_e (m_0)	0.194	0.134	0.086
m_h (m_0)	0.170	0.128	0.095
E_g (eV)	3.04	2.36	1.67

Table 3.2: Material constants of studied 3D perovskites [2].

4

Exciton Landscape

Due to the spin degeneracy of the perovskite bands the solution of Eq. (2.6) gives a fourfold degeneracy of each state. By considering a general two-particle interaction an additional energy term, corresponding to electron-hole exchange, is found. The exchange term is dependent on the spin configuration of the states and when including this term in the Hamiltonian a hybridized exciton basis is obtained, splitting the energies according to their total angular momentum. The model presented below manages to capture the qualitative spectrum in 3D and gives a constant energy splitting. In the strict 2D limit the gray state becomes dark and the long range splitting becomes dependent on the exciton center-of-mass momentum. Further, the lowest energy state is according to the model doubly degenerate which is in contradiction to experiments [5], showing one non-degenerate energy level and three levels close to each other the predicted energy splitting is however in agreement with experiments. Unknown constants in the potential make numerical values only estimative.

4.1 Inclusion of Exchange Interaction

Equation (4.1) describes a general two particle interaction, creating electrons 1 and 2 and destroying electrons 3 and 4:

$$\begin{aligned}
 H_{cv} = \frac{1}{2} \sum_{\substack{\mathbf{k}_1, \mathbf{k}_2, \mathbf{k}_3, \mathbf{k}_4 \\ s_1, s_2, s_3, s_4}} & V_{v, \mathbf{k}_3, s_3; c, \mathbf{k}_4, s_4}^{c, \mathbf{k}_1, s_1; v, \mathbf{k}_2, s_2} c_{\mathbf{k}_1, s_1}^\dagger v_{\mathbf{k}_2, s_2}^\dagger v_{\mathbf{k}_3, s_3} c_{\mathbf{k}_4, s_4} \\
 & + V_{c, \mathbf{k}_3, s_3; v, \mathbf{k}_4, s_4}^{v, \mathbf{k}_1, s_1; c, \mathbf{k}_2, s_2} v_{\mathbf{k}_1, s_1}^\dagger c_{\mathbf{k}_2, s_2}^\dagger c_{\mathbf{k}_3, s_3} v_{\mathbf{k}_4, s_4} \\
 & + V_{c, \mathbf{k}_3, s_3; v, \mathbf{k}_4, s_4}^{c, \mathbf{k}_1, s_1; v, \mathbf{k}_2, s_2} c_{\mathbf{k}_1, s_1}^\dagger v_{\mathbf{k}_2, s_2}^\dagger c_{\mathbf{k}_3, s_3} v_{\mathbf{k}_4, s_4} \\
 & + V_{v, \mathbf{k}_3, s_3; c, \mathbf{k}_4, s_4}^{v, \mathbf{k}_1, s_1; c, \mathbf{k}_2, s_2} v_{\mathbf{k}_1, s_1}^\dagger c_{\mathbf{k}_2, s_2}^\dagger v_{\mathbf{k}_3, s_3} c_{\mathbf{k}_4, s_4}.
 \end{aligned} \tag{4.1}$$

The strength of the interactions is given by the Coulomb matrix element

$$V_{m,n}^{i,j} = \langle \lambda_i \lambda_j | V | \lambda_m \lambda_n \rangle = \iint_V \Psi_i(\mathbf{r})^* \Psi_j(\mathbf{r}')^* V(\mathbf{r} - \mathbf{r}') \Psi_m(\mathbf{r}') \Psi_n(\mathbf{r}) d\mathbf{r} d\mathbf{r}', \tag{4.2}$$

where $V(\mathbf{r} - \mathbf{r}')$ is the material-specific Coulomb potential. The most probable two-particle interaction is an intraband interaction when one electron in the conduction band and one in the valance band change their momenta as described by the first two terms in Eq. (4.2) and the black arrows in Figure 4.1. Less probable and therefore considered as a correction is the interband transition (exchange interaction) when

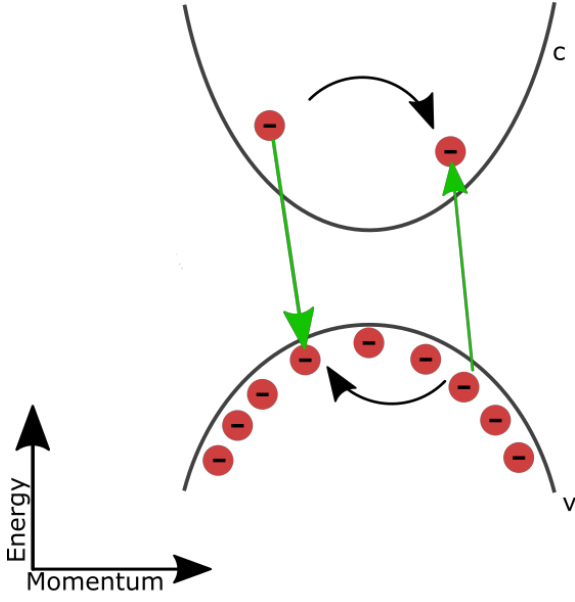


Figure 4.1: The figure shows the band structure around the band gap for the conduction and valence band in a parabolic approximation. Momentum on the x-axis and energy on the y-axis. Electrons are denoted by red circles. Black arrows indicate momentum change of electrons within bands and green the equivalent exchange process.

electrons change bands, described by the two last terms in Eq. (4.2) and green arrows in Figure 4.1. When deriving Eq. (2.6) the exchange interaction is therefore disregarded.

Changing the order of the valence and conduction band operators in the second and fourth term and interchanging 1 and 2 as well as 3 and 4 in the same terms, gives

$$H_{cv} = \sum_{\substack{\mathbf{k}_1, \mathbf{k}_2, \mathbf{k}_3, \mathbf{k}_4 \\ s_1, s_2, s_3, s_4}} c_{\mathbf{k}_1, s_1}^\dagger v_{\mathbf{k}_2, s_2}^\dagger v_{\mathbf{k}_3, s_3} c_{\mathbf{k}_4, s_4} V_{v, \mathbf{k}_3, s_3; c, \mathbf{k}_4, s_4}^{c, \mathbf{k}_1, s_1; v, \mathbf{k}_2, s_2} + c_{\mathbf{k}_1, s_1}^\dagger v_{\mathbf{k}_2, s_2}^\dagger c_{\mathbf{k}_3, s_3} v_{\mathbf{k}_4, s_4} V_{c, \mathbf{k}_3, s_3; v, \mathbf{k}_4, s_4}^{c, \mathbf{k}_1, s_1; v, \mathbf{k}_2, s_2} \quad (4.3)$$

where the relation $V_{34}^{12} = V_{43}^{21}$ has been used.

The matrix elements are evaluated using Bloch functions

$$\Psi_{a, \mathbf{k}, s}(\mathbf{r}) = \frac{1}{\sqrt{N}} e^{i\mathbf{k} \cdot \mathbf{r}} u_{a, \mathbf{k}, s}(\mathbf{r}) \quad (4.4)$$

and by Fourier transforming the potential

$$V(\mathbf{r}) = \sum_{\mathbf{q}} V_{\mathbf{q}} e^{i\mathbf{q} \cdot \mathbf{r}}. \quad (4.5)$$

The matrix element is then given by

$$\begin{aligned}
 V_{b_3 b_4}^{b_1 b_2} &= \iint_V \Psi_{b_1}(\mathbf{r})^* \Psi_{b_2}(\mathbf{r}')^* V(\mathbf{r} - \mathbf{r}') \Psi_{b_3}(\mathbf{r}') \Psi_{b_4}(\mathbf{r}) d\mathbf{r} d\mathbf{r}' \\
 &= \frac{1}{N^2} \sum_q \iint_V e^{i(-\mathbf{k}_1 + \mathbf{k}_4 + \mathbf{q}) \cdot \mathbf{r}} u_{b_1}^*(\mathbf{r}) u_{b_4}(\mathbf{r}) e^{i(-\mathbf{k}_2 + \mathbf{k}_3 - \mathbf{q}) \cdot \mathbf{r}'} u_{b_2}^*(\mathbf{r}') u_{b_3}(\mathbf{r}') V_q d\mathbf{r} d\mathbf{r}' \\
 &= \frac{1}{N^2} \sum_{q, \mathbf{R}, \mathbf{R}'} \iint_{\text{u.c.}} u_{b_1}^*(\mathbf{r}) u_{b_4}(\mathbf{r}) u_{b_2}^*(\mathbf{r}') u_{b_3}(\mathbf{r}') \times \\
 &\quad e^{i(-\mathbf{k}_1 + \mathbf{k}_4 + \mathbf{q}) \cdot (\mathbf{r} + \mathbf{R})} e^{i(-\mathbf{k}_2 + \mathbf{k}_3 - \mathbf{q}) \cdot (\mathbf{r}' + \mathbf{R}')} V_q d\mathbf{r} d\mathbf{r}' \\
 &= \frac{1}{N^2} \sum_{q, \mathbf{R}, \mathbf{R}'} \langle u_{b_1} | e^{i(-\mathbf{k}_1 + \mathbf{k}_4 + \mathbf{q}) \cdot (\mathbf{r} + \mathbf{R})} | u_{b_4} \rangle \langle u_{b_2} | e^{i(-\mathbf{k}_2 + \mathbf{k}_3 - \mathbf{q}) \cdot (\mathbf{r}' + \mathbf{R}')} | u_{b_3} \rangle V_q,
 \end{aligned} \tag{4.6}$$

where the generalized notation $b_i = \lambda_{\mathbf{k}_i, s_i}$ with $\lambda = c, v$ has been used. In the third line the integral over the whole volume has been written as a sum of integrals, each integral over one unit cell. Note that $\sum_{\mathbf{R}} e^{i(-\mathbf{k}_1 + \mathbf{k}_4 + \mathbf{q}) \cdot \mathbf{R}} d\mathbf{r} = N \sum_{\mathbf{G}} \delta_{-\mathbf{k}_1 + \mathbf{k}_4 + \mathbf{q}, \mathbf{G}}$ where \mathbf{G} is a reciprocal lattice vector, since otherwise the different contributions to the sum are canceling each other; applying this relation the matrix element may be written as

$$V_{b_3 b_4}^{b_1 b_2} = \sum_{q, \mathbf{G}, \mathbf{G}'} \langle u_{b_1} | e^{i\mathbf{G} \cdot \mathbf{r}} | u_{b_4} \rangle \langle u_{b_2} | e^{i\mathbf{G}' \cdot \mathbf{r}'} | u_{b_3} \rangle \delta_{q, \mathbf{G} + \mathbf{k}_1 - \mathbf{k}_4} \delta_{q, -\mathbf{G}' - \mathbf{k}_2 + \mathbf{k}_3} V_q. \tag{4.7}$$

For the first term in Equation (4.3), no umklapp scattering, i.e., $\mathbf{G} = 0$, is assumed which gives the leading term

$$\begin{aligned}
 &\sum_{\substack{\mathbf{k}_1, \mathbf{k}_2, \mathbf{k}_3, \mathbf{k}_4 \\ s_1, s_2, s_3, s_4}} c_{\mathbf{k}_1, s_1}^\dagger v_{\mathbf{k}_2, s_2}^\dagger v_{\mathbf{k}_3, s_3} c_{\mathbf{k}_4, s_4} V_{v, \mathbf{k}_3, s_3; c, \mathbf{k}_4, s_4}^{c, \mathbf{k}_1, s_1; v, \mathbf{k}_2, s_2} \\
 &= \sum_{\substack{\mathbf{k}_1, \mathbf{k}_2, \mathbf{k}_3, \mathbf{k}_4, \mathbf{q} \\ s_1, s_2, s_3, s_4}} \langle u_{c\mathbf{k}_4 + \mathbf{q}, s_1} | u_{c\mathbf{k}_4, s_4} \rangle \langle u_{v\mathbf{k}_3 - \mathbf{q}, s_2} | u_{v\mathbf{k}_3, s_3} \rangle V_q c_{\mathbf{k}_4 + \mathbf{q}, s_1}^\dagger v_{\mathbf{k}_3 - \mathbf{q}, s_2}^\dagger v_{\mathbf{k}_3, s_3} c_{\mathbf{k}_4, s_4}
 \end{aligned} \tag{4.8}$$

Approximating $\mathbf{q} \approx 0$ for the overlaps gives $\langle u_{\lambda\mathbf{k}, s} | u_{\mathbf{k}, s'} \rangle = \delta_{s, s'}$, which recovers the four-operator term in Eq. (2.2).

The second term in Eq. (4.3) can be divided into two qualitatively different parts — the long range part $\mathbf{G} = 0$ and the short range part $\mathbf{G} \neq 0$. Note that short-range and long-range refers to the position space and is opposite to the magnitude of the corresponding momentum vectors. The long-range $\mathbf{G} = 0$ part is

$$\begin{aligned}
 V^{\text{LR}} &= \sum_{\substack{\mathbf{k}_1, \mathbf{k}_2, \mathbf{k}_3, \mathbf{k}_4 \\ s_1, s_2, s_3, s_4}} V_{c, \mathbf{k}_3, s_3; v, \mathbf{k}_4, s_4}^{c, \mathbf{k}_1, s_1; v, \mathbf{k}_2, s_2} (\text{LR}) c_{\mathbf{k}_1, s_1}^\dagger v_{\mathbf{k}_2, s_2}^\dagger c_{\mathbf{k}_3, s_3} v_{\mathbf{k}_4, s_4} \\
 &= \sum_{\substack{\mathbf{k}_1, \mathbf{k}_2, \mathbf{k}_3, \mathbf{k}_4 \\ s_1, s_2, s_3, s_4}} \langle u_{c\mathbf{k}_1, s_1} | u_{v\mathbf{k}_4, s_4} \rangle \langle u_{v\mathbf{k}_2, s_2} | u_{c\mathbf{k}_3, s_3} \rangle V_q \delta_{\mathbf{k}_1, \mathbf{q} + \mathbf{k}_4} \delta_{\mathbf{k}_2, -\mathbf{q} + \mathbf{k}_3} c_{\mathbf{k}_1, s_1}^\dagger v_{\mathbf{k}_2, s_2}^\dagger c_{\mathbf{k}_3, s_3} v_{\mathbf{k}_4, s_4} \\
 &= \sum_{\substack{\mathbf{k}_3, \mathbf{k}_4, \mathbf{q} \\ s_1, s_2, s_3, s_4}} \langle u_{c\mathbf{k}_4 + \mathbf{q}, s_1} | u_{v\mathbf{k}_4, s_4} \rangle \langle u_{v\mathbf{k}_3 - \mathbf{q}, s_2} | u_{c\mathbf{k}_3, s_3} \rangle V_q c_{\mathbf{k}_4 + \mathbf{q}, s_1}^\dagger v_{\mathbf{k}_3 - \mathbf{q}, s_2}^\dagger c_{\mathbf{k}_3, s_3} v_{\mathbf{k}_4, s_4},
 \end{aligned} \tag{4.9}$$

which will be further evaluated through perturbation theory.

For the short-range part it holds that $\mathbf{G}, \mathbf{G}' \gg \mathbf{k}_1 - \mathbf{k}_4, -\mathbf{k}_2 + \mathbf{k}_3$ since \mathbf{k} is around the Γ point. Then $\mathbf{q} = \mathbf{G} + \mathbf{k}_1 - \mathbf{k}_4 = -\mathbf{G}' - \mathbf{k}_2 + \mathbf{k}_3$, due to the different orders of magnitude, which enforces $\mathbf{G}' = -\mathbf{G}$. By rewriting $\mathbf{q} = \mathbf{G} + \mathbf{q}'$ with small \mathbf{q}' the condition $\mathbf{q}' = \mathbf{k}_1 - \mathbf{k}_4 = -\mathbf{k}_2 + \mathbf{k}_3$ is obtained and the expression for the short-range terms looks like

$$\begin{aligned} V^{\text{SR}} &= \sum_{\substack{\mathbf{k}_1, \mathbf{k}_2, \mathbf{k}_3, \mathbf{k}_4 \\ s_1, s_2, s_3, s_4}} V_{c, \mathbf{k}_3, s_3; v, \mathbf{k}_4, s_4}^{c, \mathbf{k}_1, s_1; v, \mathbf{k}_2, s_2} (\text{SR}) c_{\mathbf{k}_1, s_1}^\dagger v_{\mathbf{k}_2, s_2}^\dagger c_{\mathbf{k}_3, s_3} v_{\mathbf{k}_4, s_4} \\ &= \sum_{\substack{\mathbf{k}_3, \mathbf{k}_4 \\ s_1, s_2, s_3, s_4 \\ \mathbf{q}', \mathbf{G}}} \langle u_{c_{\mathbf{k}_4 + \mathbf{q}', s_1}} | e^{i\mathbf{G} \cdot \mathbf{r}} | u_{v_{\mathbf{k}_4, s_4}} \rangle \langle u_{v_{\mathbf{k}_3 - \mathbf{q}, s_2}} | e^{-i\mathbf{G} \cdot \mathbf{r}'} | u_{c_{\mathbf{k}_3, s_3}} \rangle \times \\ &\quad V_{\mathbf{G} + \mathbf{q}'} c_{\mathbf{k}_4 + \mathbf{q}, s_1}^\dagger v_{\mathbf{k}_3 - \mathbf{q}, s_2}^\dagger c_{\mathbf{k}_3, s_3} v_{\mathbf{k}_4, s_4}. \end{aligned} \quad (4.10)$$

The short-range term can be further approximated by assuming $\mathbf{q}' = 0$ in the Bloch functions and $V_{\mathbf{G} + \mathbf{q}'} = V_{\mathbf{G}}$. Note that $V_{\mathbf{G}} \propto \frac{1}{NV_{\text{u.c.}}}$ and that the N is moved out. Further it is possible to Taylor expand $e^{i\mathbf{G} \cdot \mathbf{r}} \approx 1 + i\mathbf{G} \cdot \mathbf{r}$. By using the relation

$$\langle 1 | \{H, \mathbf{r}\} | 2 \rangle = (E_1 - E_2) \langle 1 | \mathbf{r} | 2 \rangle = \langle 1 | \frac{1}{2m_0} \times 2i\hat{\mathbf{p}}\hbar | 1 \rangle \quad (4.11)$$

the expression for the short-range parts is simplified to (note that the operators are omitted for shortness but remain unchanged)

$$V^{\text{SR}} = \frac{1}{NE_g^2} \sum_{\substack{\mathbf{k}_3, \mathbf{k}_4, \mathbf{G}, \mathbf{q} \\ s_1, s_2, s_3, s_4}} \langle u_{c_{\mathbf{k}_4, s_1}} | 1 + i\mathbf{G} \cdot \frac{\hbar\hat{\mathbf{p}}}{m_0} | u_{v_{\mathbf{k}_4, s_4}} \rangle \langle u_{v_{\mathbf{k}_3, s_2}} | 1 - i\mathbf{G} \cdot \frac{\hbar\hat{\mathbf{p}}}{m_0} | u_{c_{\mathbf{k}_3, s_3}} \rangle V_{\mathbf{G}}, \quad (4.12)$$

which can be further evaluated through perturbation theory and assuming a form for the Bloch factors u .

4.2 Perturbation

For evaluating the overlaps in Eq. (4.9) and terms of the form $\mathbf{d}_{ss'}^{\lambda\lambda'} = \langle \lambda s | \hat{\mathbf{p}} | \lambda' s' \rangle$ in Eq. (4.12), perturbation theory may be used. In perturbation theory a disturbance is added to the ground state Hamiltonian which results in changes of the wavefunctions and energies. The results received when applying perturbation are presented here, while the details can be found in Appendix A.

In the overlaps, Eq. (4.9), of the form $\langle u_{c_{\mathbf{k} + \mathbf{q}, s}} | u_{v_{\mathbf{k}, s'}} \rangle$, the \mathbf{q} is small and can be treated as a perturbation. To first order the overlap is then given by

$$\langle u_{c_{\mathbf{k} + \mathbf{q}, s}} | u_{v_{\mathbf{k}, s'}} \rangle = \langle u_{v_{\mathbf{k} - \mathbf{q}, s'}} | u_{c_{\mathbf{k}, s}} \rangle^* = \frac{\hbar\mathbf{q}}{m_0} \cdot \frac{\langle u_{c_{\mathbf{k}s}} | \hat{\mathbf{p}} | u_{v_{\mathbf{k}s'}} \rangle}{E_{c\mathbf{k}} - E_{v\mathbf{k}}} = \frac{\hbar}{m_0 E_g} \mathbf{q} \cdot \mathbf{d}_{ss'}^{cv} \quad (4.13)$$

where the $\mathbf{d}_{ss'}^{\lambda\lambda'}$ terms once more turn up. To evaluate these the energy is further approximated to second order as

$$E_{n\mathbf{k}} = \frac{1}{2} E_g + \frac{\hbar^2 \mathbf{k}^2}{2m_0} + \left(\frac{\hbar\mathbf{k} | \mathbf{d}_{s, \bar{s}}^{\lambda, \lambda'} |}{m_0} \right)^2 \frac{1}{\Delta_{\lambda, \lambda'}} \quad (4.14)$$

where $\Delta_{\lambda,\lambda'} = E_{\lambda\mathbf{k}} - E_{\lambda'\mathbf{k}}$. By making a harmonic approximation the energy can also be expressed as

$$E_{n\mathbf{k}} = \frac{1}{2}E_g + \frac{\hbar^2\mathbf{k}^2}{2m_e} \quad (4.15)$$

with m_e the effective mass of the electron. Putting the two expressions equal to each other gives

$$\frac{1}{2}E_g + \frac{\hbar^2\mathbf{k}^2}{2m_0} + \left(\frac{\hbar\mathbf{k}|\mathbf{d}_{s,\bar{s}}^{\lambda,\lambda'}|}{m_0}\right)^2 \frac{1}{\Delta_{\lambda,\lambda'}} = \frac{1}{2}E_g + \frac{\hbar^2\mathbf{k}^2}{2m_\lambda} \quad (4.16)$$

with the solution for d

$$|\mathbf{d}_{s,\bar{s}}^{\lambda,\lambda'}|^2 = \frac{m_0\Delta_{\lambda,\lambda'}}{2} \left(\frac{m_0}{m_\lambda} - 1\right), \quad (4.17)$$

note that there is no dependence on s , $|\mathbf{d}^{\lambda,\lambda'}|^2 = |\mathbf{d}^{\lambda',\lambda}|^2$, $\Delta_{\lambda,\lambda'} = -\Delta_{\lambda',\lambda}$ and that consideration of all directions gives a dimensional factor c equal to the dimensionality of the system

$$c|\mathbf{d}^{\lambda,\lambda'}|^2 = \frac{c}{2}(|\mathbf{d}^{\lambda,\lambda'}|^2 + |\mathbf{d}^{\lambda',\lambda}|^2) = \frac{m_0^2\Delta_{\lambda,\lambda'}}{2} \left(\frac{1}{m_\lambda} - \frac{1}{m_{\lambda'}}\right), \quad (4.18)$$

which yields

$$d^{cv} = \sqrt{\frac{m_0^2 E_g}{c} \frac{1}{m_\mu}} \quad (4.19)$$

with m_μ the reduced mass of the exciton. Note that the expression in Eq. (4.19) is independent of momentum.

4.3 Effect of Spin Orbit Coupling

In the perovskites of interest in this work, spin orbit coupling gives rise to mixing of spatial P orbitals and spin in conduction band, while leaving the S orbitals in the valence band unmixed. Assuming cubic symmetry, the Bloch factors are given by (note no momentum dependence)

$$\begin{aligned} |u_{c\mathbf{k}s}\rangle &= |cs\rangle = \frac{1}{\sqrt{3}}(-|P_x\bar{s}\rangle - i\sigma_s|P_y\bar{s}\rangle - \sigma_s|P_zs\rangle) \\ |u_{v\mathbf{k}s}\rangle &= |vs\rangle = |Ss\rangle \end{aligned} \quad (4.20)$$

where \bar{s} denotes the opposite spin of s and σ_s is 1 if s is up and -1 if s is down; see also Eq. (3.1) [16].

When applying the Bloch functions in Eq. (4.12) the constant terms vanish since there is no overlap between S and P orbitals $\langle S|P\rangle = 0$. Then only factors of

the form $\mathbf{G} \cdot \langle vs | \hat{\mathbf{p}} | cs' \rangle$ remain which may be expanded as (using a general vector $\mathbf{A} \in \mathbf{q}, \mathbf{G}$)

$$\begin{aligned} \mathbf{A} \cdot \langle vs | \hat{\mathbf{p}} | cs' \rangle &= \mathbf{A} \cdot \frac{1}{\sqrt{3}} \left[-\delta_{s,s'} \sigma_{s'} \langle Ss | \hat{\mathbf{p}} | P_z s' \rangle \right. \\ &\quad \left. - \delta_{s,\bar{s}'} (\langle Ss | \hat{\mathbf{p}} | P_x s' \rangle + i \sigma_{s'} \langle Ss | \hat{\mathbf{p}} | P_y s' \rangle) \right], \end{aligned}$$

the same holds for the long-range term but then $\mathbf{A} = \mathbf{q}$.

It is possible to further simplify the expression by considering the direction of the dipole matrix elements. The direction is given by the momentum operator which is in turn given by the nabla operator. The P_i and S orbitals have angular symmetry equal to that of the corresponding hydrogenic wavefunctions. Evaluating the angular parts of the overlaps gives $\langle S | \hat{\mathbf{p}} | P_i \rangle = \hat{i}$ (see Appendix B for a detailed calculation) which leads to

$$\mathbf{A} \cdot \langle vs | \hat{\mathbf{p}} | cs' \rangle = \frac{d}{\sqrt{3}} \left[-\delta_{s,s'} \sigma_{s'} A_z - \delta_{s,\bar{s}'} (A_x + i \sigma_{s'} A_y) \right] \quad (4.21)$$

and

$$V^{\text{LR}} + V^{\text{SR}} = \sum_{\substack{\mathbf{k}_3, \mathbf{k}_4, \mathbf{q}, \mathbf{G} \\ s_1, s_2, s_3, s_4}} (M_{s_3, s_2}^{s_1, s_4}(\mathbf{G}) V_{\mathbf{G}} + M_{s_3, s_2}^{s_1, s_4}(\mathbf{q}) V_{\mathbf{q}}) c_{\mathbf{k}_4 + \mathbf{q}, s_1}^\dagger v_{\mathbf{k}_3 - \mathbf{q}, s_2}^\dagger c_{\mathbf{k}_3, s_3} v_{\mathbf{k}_4, s_4} \quad (4.22)$$

where

$$\begin{aligned} M_{s_3, s_2}^{s_1, s_4}(\mathbf{A}) &= \frac{\hbar^2 d^2}{3N E_g^2 m_0^2} \left[\delta_{s_2, s_3} \sigma_{s_3} A_z + \delta_{s_2 + s_3, 0} (A_x + i \sigma_{s_3} A_y) \right] \times \\ &\quad \left[\delta_{s_1, s_4} \sigma_{s_1} A_z + \delta_{s_1 + s_4, 0} (A_x - i \sigma_{s_1} A_y) \right] \end{aligned} \quad (4.23)$$

and d^2 is given by Eq. (4.19).

4.4 Exciton States

To add the exchange term Eq. (4.3) to Eq. (2.6), the terms need to be written in the same exciton basis. The electron operators are rewritten

$$\begin{aligned} c_{\mathbf{k}_4 + \mathbf{q}, s_1}^\dagger v_{\mathbf{k}_3 - \mathbf{q}, s_2}^\dagger c_{\mathbf{k}_3, s_3} v_{\mathbf{k}_4, s_4} &= -c_{\mathbf{k}_4 + \mathbf{q}, s_1}^\dagger v_{\mathbf{k}_3 - \mathbf{q}, s_2}^\dagger v_{\mathbf{k}_4, s_4} c_{\mathbf{k}_3, s_3} \\ &= c_{\mathbf{k}_4 + \mathbf{q}, s_1}^\dagger (v_{\mathbf{k}_4, s_4} v_{\mathbf{k}_3 - \mathbf{q}, s_2}^\dagger - \delta_{\mathbf{k}_4, \mathbf{k}_3 - \mathbf{q}} \delta_{s_2, s_4}) c_{\mathbf{k}_3, s_3} \end{aligned}$$

where the two-operator term is disregarded and the relations in Eq. (2.4) are used to transform into the exciton basis

$$c_{\mathbf{k}_4 + \mathbf{q}, s_1}^\dagger v_{\mathbf{k}_4, s_4} v_{\mathbf{k}_3 - \mathbf{q}, s_2}^\dagger c_{\mathbf{k}_3, s_3} = \sum_{\nu, \mu} \phi_{\mathbf{k}_4 + \alpha_h \mathbf{q}}^\nu \phi_{\mathbf{k}_3 - \alpha_e \mathbf{q}}^{\mu*} X_{\mathbf{q}}^{\nu s_1 s_4 \dagger} X_{\mathbf{q}}^{\mu s_3 s_2}. \quad (4.24)$$

Combining this with Eq. (2.6) yields the full expression for the Hamiltonian

$$\begin{aligned} H &= \sum_{\mathbf{q}, \nu, s, s'} \left(\frac{\hbar^2 \mathbf{q}^2}{2M} + E^\nu \right) X_{\mathbf{q}}^{\nu s s' \dagger} X_{\mathbf{q}}^{\nu s s'} \\ &\quad + \sum_{\substack{\mathbf{k}_3, \mathbf{k}_4, \mathbf{q}, \mathbf{G} \\ s_1, s_2, s_3, s_4 \\ \nu, \mu}} (M_{s_3, s_2}^{s_1, s_4}(\mathbf{G}) V_{\mathbf{G}} + M_{s_3, s_2}^{s_1, s_4}(\mathbf{q}) V_{\mathbf{q}}) \phi_{\mathbf{k}}^\nu \phi_{\mathbf{k}'}^{\mu*} X_{\mathbf{q}}^{\nu s_1 s_4 \dagger} X_{\mathbf{q}}^{\mu s_3 s_2}. \end{aligned} \quad (4.25)$$

When including the exchange interaction, the exciton basis X is no longer diagonalizing the Hamiltonian and a new hybridized basis including spin needs to be used. The hybridized basis is

$$\begin{aligned} X_{\mathbf{q}}^{ss'\dagger} &= \sum_n \theta_{n\mathbf{q}}^{ss'} Y_{n\mathbf{q}}^\dagger \\ X_{\mathbf{q}}^{ss'} &= \sum_n \theta_{n\mathbf{q}}^{ss'*} Y_{n\mathbf{q}}. \end{aligned}$$

Applying the new basis, from now on only including states $\mu = \nu = 1s$, since only the lowest energies are regarded, the Hamiltonian becomes

$$\begin{aligned} H &= \sum_{\mathbf{q}, s, s'} \left(\frac{\hbar^2 \mathbf{q}^2}{2M} + E^{1s} \right) \sum_n \theta_{n\mathbf{q}}^{ss'} Y_{n\mathbf{q}}^\dagger \sum_{n'} \theta_{n'\mathbf{q}}^{ss'*} Y_{n'\mathbf{q}} \\ &\quad + \sum_{\substack{\mathbf{k}, \mathbf{k}', \mathbf{q}, \mathbf{G} \\ s_1, s_2, s_3, s_4}} (M_{s_3, s_2}^{s_1, s_4}(\mathbf{G}) V_{\mathbf{G}} + M_{s_3, s_2}^{s_1, s_4}(\mathbf{q}) V_{\mathbf{q}}) \phi_{\mathbf{k}}^{1s} \phi_{\mathbf{k}'}^{1s*} \sum_n \theta_{n\mathbf{q}}^{s_1, s_4} Y_{n\mathbf{q}}^\dagger \sum_{n'} \theta_{n'\mathbf{q}}^{s_3, s_2*} Y_{n'\mathbf{q}} \\ &= \sum_{\substack{\mathbf{q} \\ s_2, s_3 \\ n, n'}} [E(\mathbf{q}) \theta_{n\mathbf{q}}^{s_3, s_2} \\ &\quad + \sum_{s_1, s_4, \mathbf{G}} (M_{s_3, s_2}^{s_1, s_4}(\mathbf{G}) V_{\mathbf{G}} + M_{s_3, s_2}^{s_1, s_4}(\mathbf{q}) V_{\mathbf{q}}) |\phi_{(r=0)}^{1s}|^2 \theta_{n\mathbf{q}}^{s_1, s_4}] \theta_{n'\mathbf{q}}^{s_3, s_2*} Y_{n\mathbf{q}}^\dagger Y_{n'\mathbf{q}} \\ &= \sum_{\mathbf{q}, n, n', s_3, s_2} \epsilon_{n\mathbf{q}} \theta_{n\mathbf{q}}^{s_3, s_2} \theta_{n'\mathbf{q}}^{s_3, s_2*} Y_{n\mathbf{q}}^\dagger Y_{n'\mathbf{q}}. \end{aligned}$$

Where $\sum_{\mathbf{k}} \phi_{\mathbf{k}}^{1s} = \phi_{(r=0)}^{1s} = \phi_0^{1s}$ has been used. The matrix times the potential $M_{s_3, s_2}^{s_1, s_4}(\mathbf{A}) V_{\mathbf{A}}$ written out in the θ basis is

$$\begin{aligned} \sum_{\mathbf{A}} M_{s_3, s_2}^{s_1, s_4}(\mathbf{A}) V_{\mathbf{A}} &= \frac{\hbar^2 |\phi_0^{1s}|^2}{3cN E_g m_\mu} \sum_{\mathbf{A}} V_{\mathbf{A}} \times \\ &\left(\begin{array}{c|cccc} s_3 s_2 \backslash s_1 s_4 & \uparrow\uparrow & \uparrow\downarrow & \downarrow\uparrow & \downarrow\downarrow \\ \hline \uparrow\uparrow & A_z^2 & A_z(A_x - iA_y) & A_z(A_x + iA_y) & -A_z^2 \\ \uparrow\downarrow & A_z(A_x + iA_y) & (A_x^2 + A_y^2) & (A_x + iA_y)^2 & -A_z(A_x + iA_y) \\ \downarrow\uparrow & A_z(A_x - iA_y) & (A_x - iA_y)^2 & (A_x^2 + A_y^2) & -A_z(A_x - iA_y) \\ \downarrow\downarrow & -A_z^2 & -A_z(A_x - iA_y) & A_z(A_x + iA_y) & A_z^2 \end{array} \right). \end{aligned}$$

Assuming spherical symmetry the G_x , G_y and $G_x G_y$ terms cancel and G_x^2 and G_y^2 contribute equally when summed. The same holds for \mathbf{q} , since due to the symmetry of the operators it is possible to integrate over the angular dependency, in other words $Y_{n\mathbf{q}}^\dagger$ is independent of the direction of \mathbf{q} . The expression then simplifies to

$$\sum_{\mathbf{A}} M_{s_3, s_2}^{s_1, s_4}(\mathbf{A}) V_{\mathbf{A}} = \frac{\hbar^2 |\phi_0^{1s}|^2}{3cN E_g m_\mu} \sum_{\mathbf{A}} V_{\mathbf{A}} \begin{pmatrix} A_z^2 & 0 & 0 & -A_z^2 \\ 0 & 2A_x^2 & 0 & 0 \\ 0 & 0 & 2A_x^2 & 0 \\ -A_z^2 & 0 & 0 & A_z^2 \end{pmatrix}. \quad (4.26)$$

The whole eigenvalue equation $H\Psi_{n,q} = \epsilon_{n,q}\Psi_{n,q}$ in matrix form with symmetry considered is

$$\left[EI + \frac{\hbar^2|\phi_0^{1s}|^2}{3cNE_gm_\mu} \sum_{\mathbf{G},\mathbf{A}} V_{\mathbf{A}} \begin{pmatrix} A_z^2 & 0 & 0 & -A_z^2 \\ 0 & 2A_x^2 & 0 & 0 \\ 0 & 0 & 2A_x^2 & 0 \\ -A_z^2 & 0 & 0 & A_z^2 \end{pmatrix} \right] \begin{pmatrix} \theta_{nq}^{\uparrow\uparrow} \\ \theta_{nq}^{\uparrow\downarrow} \\ \theta_{nq}^{\downarrow\uparrow} \\ \theta_{nq}^{\downarrow\downarrow} \end{pmatrix} = \epsilon_{nq} \begin{pmatrix} \theta_{nq}^{\uparrow\uparrow} \\ \theta_{nq}^{\uparrow\downarrow} \\ \theta_{nq}^{\downarrow\uparrow} \\ \theta_{nq}^{\downarrow\downarrow} \end{pmatrix}. \quad (4.27)$$

with the solutions

$$\epsilon_{1,\pm 1} = E + \frac{\hbar^2|\phi_0^{1s}|^2}{3cNE_gm_\mu} \sum_{\mathbf{G}} 2(V_{\mathbf{G}}G_x^2 + V_{\mathbf{q}}q_x^2) \quad \text{for} \quad \Psi_{1,1} = \begin{pmatrix} 0 \\ 1 \\ 0 \\ 0 \end{pmatrix} \quad \text{and} \quad \Psi_{1,-1} = \begin{pmatrix} 0 \\ 0 \\ 1 \\ 0 \end{pmatrix},$$

$$\epsilon_{1,0} = E + \frac{\hbar^2|\phi_0^{1s}|^2}{3cNE_gm_\mu} \sum_{\mathbf{G}} 2(V_{\mathbf{G}}G_z^2 + V_{\mathbf{q}}q_z^2) \quad \text{for} \quad \Psi_{1,0} = \frac{1}{\sqrt{2}} \begin{pmatrix} 1 \\ 0 \\ 0 \\ -1 \end{pmatrix}$$

and

$$\epsilon_{0,0} = E \quad \text{for} \quad \Psi_{0,0} = \frac{1}{\sqrt{2}} \begin{pmatrix} 1 \\ 0 \\ 0 \\ 1 \end{pmatrix}.$$

Note that E is negative and the shifts are all positive, making the dark state the energetically lowest one and that the first subscript in the energies and states is the total angular momentum and the second the angular momentum projected on the z -axis.

4.4.1 Characterization of States

The states are characterized by evaluating their optical matrix elements, see Eq. (2.7). When changing basis the relevant optical matrix elements transform as

$$D_n^{cv} = \sum_{ss'} \theta_{n\mathbf{Q}}^{ss'} D_{ss'}^{cv} = \sum_n \theta_{n\mathbf{Q}}^{ss'} \phi^{1s} d_{ss'}^{cv} \quad (4.28)$$

where ϕ^{1s} is the same for all transition elements and not explicitly written out in the following. The dipole matrix elements for the hybridized states are evaluated by using Eq. (4.21) with \mathbf{A} being the electromagnetic vector potential, giving

$$\begin{aligned}
 D_{0,0}^{cv} &\propto \frac{1}{\sqrt{2}}d_{\uparrow\uparrow}^{cv} + \frac{1}{\sqrt{2}}d_{\downarrow\downarrow}^{cv} = \frac{d}{\sqrt{6}}(-A_z + A_z)\hat{z} = 0 \\
 D_{1,0}^{cv} &\propto \frac{1}{\sqrt{2}}d_{\uparrow\uparrow}^{cv} - \frac{1}{\sqrt{2}}d_{\downarrow\downarrow}^{cv} = \frac{d}{\sqrt{6}}(-A_z - A_z)\hat{z} \neq 0 \\
 D_{1,1}^{cv} &\propto -d_{\downarrow\uparrow}^{cv} = \frac{d}{\sqrt{3}}(A_x\hat{x} + iA_y\hat{y}) \neq 0 \\
 D_{1,-1}^{cv} &\propto d_{\uparrow\downarrow}^{cv} = \frac{d}{\sqrt{3}}(-A_x\hat{x} + iA_y\hat{y}) \neq 0.
 \end{aligned}$$

From these results the states are characterized as $\Psi_{0,0}^{\text{dark}}$, $\Psi_{1,0}^{\text{gray}}$ and $\Psi_{1,\pm 1}^{\text{bright}}$. Note further that the polarization of the light can be used to experimentally differ between the bright states. For left (right) polarized light the relation $A_x = (-)iA_y$, $A_z = 0$ holds. It follows that $\Psi_{1,1}^{\text{bright}}$ couples to right-polarized light and $\Psi_{1,-1}^{\text{bright}}$ to left-polarized light.

4.5 Landscape in 2D

When considering the 2D case an envelope function $f(z)$ is added to the Bloch function $\Psi_{\mathbf{k}}(\mathbf{r}) = f(z)u_{\mathbf{k}\approx 0}(\mathbf{r})e^{i\mathbf{k}_{\parallel}\cdot\mathbf{r}_{\parallel}}$ [19] where \mathbf{r}_{\parallel} is the in plane position and \mathbf{k}_{\parallel} the in-plane momentum. The confinement function should mimic the confinement of the electrons. In the strict 2D limit the envelope function is chosen to be a δ -function — basically removing all z components $q_z, G_z, \langle S|\delta(z)\hat{\mathbf{p}}|P_z\rangle = 0$. In the rest of the thesis this will be the case referred to as 2D. The energy eigenvalue equation is then modified to

$$\left[E\mathbf{I} + \frac{\hbar^2|\phi_0^{1s}|^2}{3cNE_gm_{\mu}} \sum_{\mathbf{G},\mathbf{A}} V_{\mathbf{A}} \begin{pmatrix} 0 & 0 & 0 & 0 \\ 0 & 2A_x^2 & 0 & 0 \\ 0 & 0 & 2A_x^2 & 0 \\ 0 & 0 & 0 & 0 \end{pmatrix} \right] \begin{pmatrix} \theta_{nq}^{\uparrow\uparrow} \\ \theta_{nq}^{\uparrow\downarrow} \\ \theta_{nq}^{\downarrow\uparrow} \\ \theta_{nq}^{\downarrow\downarrow} \end{pmatrix} = \epsilon_{nq} \begin{pmatrix} \theta_{nq}^{\uparrow\uparrow} \\ \theta_{nq}^{\uparrow\downarrow} \\ \theta_{nq}^{\downarrow\uparrow} \\ \theta_{nq}^{\downarrow\downarrow} \end{pmatrix}. \quad (4.29)$$

With the solutions

$$\epsilon_{1,\pm 1} = E + \frac{\hbar^2|\phi_0^{1s}|^2}{3cNE_gm_{\mu}} \sum_{\mathbf{G}} 2(V_{\mathbf{G}}G_x^2 + V_{\mathbf{q}}q_x^2) \quad \text{for} \quad \Psi_{1,1} = \begin{pmatrix} 0 \\ 1 \\ 0 \\ 0 \end{pmatrix} \quad \text{and} \quad \Psi_{1,-1} = \begin{pmatrix} 0 \\ 0 \\ 1 \\ 0 \end{pmatrix}$$

and

$$\epsilon_{0,0} = E \quad \text{for} \quad \Psi_{1,0} = \frac{1}{\sqrt{2}} \begin{pmatrix} 1 \\ 0 \\ 0 \\ -1 \end{pmatrix} \quad \text{and} \quad \Psi_{0,0} = \frac{1}{\sqrt{2}} \begin{pmatrix} 1 \\ 0 \\ 0 \\ 1 \end{pmatrix}.$$

The dipole elements also change so that $\Psi_{1,0}$ changes from gray to dark, giving $\Psi_{0,0}^{\text{dark}}$, $\Psi_{1,0}^{\text{dark}}$ and $\Psi_{1,\pm 1}^{\text{bright}}$.

4.6 Value of Bright-Dark Energy Splitting

The expression for the splitting is the same (apart from c) in both dimensions $E_{\text{BD}} = \frac{\hbar^2 |\phi_0^{1s}|^2}{3cN E_g m_\mu} \sum_{\mathbf{G}} 2(V_{\mathbf{G}} G_x^2 + V_{\mathbf{q}} q_x^2)$, but its evaluation differs. The difference is the method of obtaining the wave function, what potential that is used and the dimensionality of momenta.

4.6.1 3D

In the 3D case, the energy splitting between the bright and dark states is given by

$$E_{\text{BD}} = \frac{\hbar^2 |\phi_0^{1s}|^2}{9N E_g m_\mu} \times \sum_{\mathbf{G}} 2(V_{\mathbf{G}} G_x^2 + V_{\mathbf{q}} q_x^2). \quad (4.30)$$

The potential in 3D is given by $V_{\mathbf{q}} = \frac{e^2}{\Omega \epsilon \epsilon_0 q^2}$ where Ω is the unit cell volume. Using the 3D potential the sum in the short range term can be written as $\frac{1}{N} \sum_{\mathbf{G}} \frac{2G_x^2}{G^2} = \frac{2}{3N} \sum_{\mathbf{G}} \frac{G_x^2 + G_y^2 + G_z^2}{G^2} = \frac{2}{3}$, since, assuming cubic symmetry, it holds that $\sum_{\mathbf{G}} \frac{G_x^2}{G^2} = \sum_{\mathbf{G}} \frac{G_y^2}{G^2} = \sum_{\mathbf{G}} \frac{G_z^2}{G^2}$ and $G^2 = G_x^2 + G_y^2 + G_z^2$. The sum in the long-range term can in the same way be written $\frac{1}{N} \sum_{\mathbf{G}} \frac{2q_x^2}{q^2} = \frac{2}{3} \frac{q_x^2 + q_y^2 + q_z^2}{q^2} = \frac{2}{3}$, still assuming cubic symmetry. So in total, the bright-dark splitting is

$$E_{\text{BD}} = 2 \frac{2\hbar^2 |\phi_0^{1s}|^2 e^2}{27 E_g \epsilon \epsilon_0 m_\mu}. \quad (4.31)$$

Further, $|\phi_0^{1s}|^2 = \frac{V}{\pi a_b^3}$ in 3D where a_b is the Bohr radius given by $a_b = \frac{4\pi \epsilon \epsilon_0 \hbar^2}{m_\mu e^2}$ [2] and V is the volume of the sample¹. Using the material constants in Table 3.2 the energy splitting is evaluated for three cubic perovskites, the values are presented in Table 4.1 and are within one order of magnitude of values found in literature [2].

Perovskite	Bright-dark splitting E_{BD} (meV)
CsPbCl ₃	2.89
CsPbBr ₃	1.50
CsPbI ₃	0.86

Table 4.1: Bright-dark energy splitting for three cubic 3D perovskites according to Eq. (4.31).

4.6.2 2D

In the 2D case, the energy splitting between the bright and dark states is given by

$$E_{\text{BD}} = \frac{\hbar^2 |\phi_0^{1s}|^2}{6N E_g m_\mu} \sum_{\mathbf{G}} 2(V_{\mathbf{G}} G_x^2 + V_{\mathbf{q}} q_x^2). \quad (4.32)$$

¹Note that there is a factor $\frac{V}{\Omega} = N$ that is not accounted for. However, the numerical result should not be dependent on the size of the sample. A similar problem arises in 2D.

For the long range (small \mathbf{q}) part the potential $V_{\mathbf{q}} = \frac{e^2}{2\epsilon\epsilon_{\text{well}}Aq(1+r_0q)}$ with $r_0 = L_{\text{well}}\frac{\epsilon_{\text{well}}}{2\epsilon_{\text{org}}}$ is used in 2D [3]. The same potential is used when solving the Wannier equation for getting the wave function $|\phi_0^{1s}|^2$ since that is done for small \mathbf{q} . The long-range splitting is thus \mathbf{q} dependent and is explicitly

$$E_{\text{BD}}^{\text{LR}} = \frac{\hbar^2|\phi_0^{1s}|^2}{6E_g m_\mu} \frac{qe^2}{2\epsilon\epsilon_{\text{well}}A(1+r_0q)} \quad (4.33)$$

where $q_x^2 + q_y^2 = q^2$ has been used. For the short range (large \mathbf{q}) the potential behaves differently and is given by $V_{\mathbf{q}} = \frac{e^2}{\Omega\epsilon\epsilon_0q^2}$ [20]. In this work the dielectric constant, ϵ , is taken as that of the dielectric medium. With this potential the sum $\frac{1}{N}\sum_{\mathbf{G}}\frac{G_x^2+G_y^2}{G^2} = 1$ since $G^2 = G_x^2 + G_y^2$ and the splitting is constant and given by

$$E_{\text{BD}} = \frac{\hbar^2|\phi_0^{1s}|^2e^2}{6E_g\epsilon\epsilon_0m_\mu}. \quad (4.34)$$

Using the material constants from Table 3.1, the constant short-range splitting is found to be 25.39 meV in PEA_2PbI_4 comparable to experiments [5]. The total energy dispersion and the long-range and short-range part energies for different COM are separately shown in Figure 4.2. The short-range part is governing the overall behavior and the long-range part is vanishing for small COM. Note that the momentum range for the long-range part is much smaller than in the other plots to capture the behavior around zero momentum.

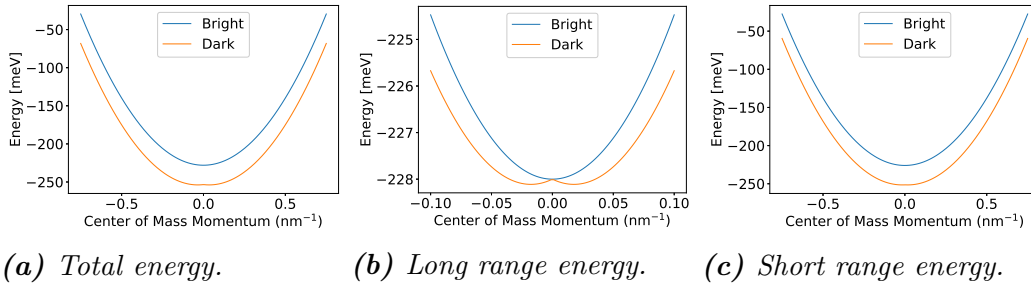


Figure 4.2: Total energy and short and long range energies for PEA_2PbI_4 .

5

Magnetic Field

In the presence of a magnetic field the symmetry of the system will change, mixing the hybridized exciton states $\Psi_{\alpha,\beta}$ of the non magnetic field case, and changing the energies. Qualitatively important is that the degeneracies will be broken. The energies in 2D are, however, still not in accordance with experiments [5]. In this chapter the magnetically modified Hamiltonian is derived and the magnetically modified states are qualitatively and quantitatively described.

Mathematically the effect of the magnetic field is seen by the emergence of magnetic field dependent terms in the Hamiltonian. The diagonal elements are neglected. Note that, as mentioned in section 2.2, only an in plane magnetic field is considered. In the hybridized base, the magnetic Hamiltonian see Eq. (2.15) is

$$H_{el-mag} = \sum_{\substack{\vec{k}, \vec{q} \\ s_1, s_2, s_3, s_4}} \frac{B\mu_B}{2} (g^c \delta_{s_2, s_4} \delta_{s_1, \bar{s}_3} - g^v \delta_{s_2, \bar{s}_4} \delta_{s_1, s_3}) \theta_{n\vec{q}}^{s_1, s_4} \theta_{n'\vec{q}}^{s_3, s_2*} Y_{n\vec{q}}^\dagger Y_{n'\vec{q}}, \quad (5.1)$$

note that since only 1s states are considered ($\mu = \nu = 1s$) that $\sum_{\vec{k}} \phi_{\vec{k}}^\nu \phi_{\vec{k}}^{\mu*} = 1$. On matrix form in the hybridized basis the magnetic Hamiltonian is

$$H_{el-mag} = \frac{B\mu_B}{2} \begin{pmatrix} 0 & -g^v & g^c & 0 \\ -g^v & 0 & 0 & g^c \\ g^c & 0 & 0 & -g^v \\ 0 & -g^v & g^c & 0 \end{pmatrix}. \quad (5.2)$$

To easier appreciate how the magnetic elements affect the hybridized eigenstates, it is advantageous to express the Hamiltonian in the basis of eigenstates in the absence of a magnetic field $\Psi_{\alpha,\beta}$. Then the matrix becomes

$$H_{el-mag} = \frac{B\mu_B}{2\sqrt{2}} \begin{pmatrix} & \Psi_{1,1}^{\text{bright}} & \Psi_{1,-1}^{\text{bright}} & \Psi_{1,0}^{\text{dark/gray}} & \Psi_{0,0}^{\text{dark}} \\ \Psi_{1,1}^{\text{bright}} & 0 & 0 & -g_T & g_L \\ \Psi_{1,-1}^{\text{bright}} & 0 & 0 & g_T & g_L \\ \Psi_{1,0}^{\text{dark/gray}} & -g_T & g_T & 0 & 0 \\ \Psi_{0,0}^{\text{dark}} & g_L & g_L & 0 & 0 \end{pmatrix}, \quad (5.3)$$

where $g_L = g^c - g^v$ and $g_T = g^c + g^v$. The Hamiltonian in Eq. (5.3) mixes the bright states with the gray and dark respectively. There is no mixing between gray and dark states.

Writing the full Hamiltonian, Eqs. (4.27) and (4.29), in the same basis gives

$$H = \begin{pmatrix} \epsilon_{1,1} & 0 & -\frac{B\mu_B}{2\sqrt{2}}g_T & \frac{B\mu_B}{2\sqrt{2}}g_L \\ 0 & \epsilon_{1,-1} & \frac{B\mu_B}{2\sqrt{2}}g_T & \frac{B\mu_B}{2\sqrt{2}}g_L \\ -\frac{B\mu_B}{2\sqrt{2}}g_T & \frac{B\mu_B}{2\sqrt{2}}g_T & \epsilon_{1,0} & 0 \\ \frac{B\mu_B}{2\sqrt{2}}g_L & \frac{B\mu_B}{2\sqrt{2}}g_L & 0 & \epsilon_{0,0} \end{pmatrix}. \quad (5.4)$$

Solving the eigenvalue problem gives the energies and states as a function of magnetic field. The energy levels are

$$E_L^\pm = \frac{1}{2} \left(\epsilon_{0,0} + \epsilon_{1,\pm 1} \pm \sqrt{(\epsilon_{0,0} - \epsilon_{1,\pm 1})^2 + (B\mu_B g_L)^2} \right) \quad (5.5)$$

and

$$E_T^\pm = \frac{1}{2} \left(\epsilon_{1,0} + \epsilon_{1,\pm 1} \pm \sqrt{(\epsilon_{1,0} - \epsilon_{1,\pm 1})^2 + (B\mu_B g_T)^2} \right), \quad (5.6)$$

with the eigenstates

$$\Psi_L^\pm = \frac{1}{N_{(0,0),L}^\pm} \begin{pmatrix} 1 \\ 1 \\ 0 \\ \frac{\sqrt{2}}{B\mu_B g_L} \left(\epsilon_{0,0} - \epsilon_{1,\pm 1} \pm \sqrt{(\epsilon_{0,0} - \epsilon_{1,\pm 1})^2 + (B\mu_B g_L)^2} \right) \end{pmatrix} = \begin{pmatrix} \phi_{L,1,1}^\pm \\ \phi_{L,1,1}^\pm \\ 0 \\ \phi_{L,0,0}^\pm \end{pmatrix} \quad (5.7)$$

and

$$\Psi_T^\pm = \frac{1}{N_{(1,0),T}^\pm} \begin{pmatrix} 1 \\ -1 \\ -\frac{\sqrt{2}}{B\mu_B g_T} \left(\epsilon_{1,0} - \epsilon_{1,\pm 1} \pm \sqrt{(\epsilon_{1,0} - \epsilon_{1,\pm 1})^2 + (B\mu_B g_T)^2} \right) \\ 0 \end{pmatrix} = \begin{pmatrix} \phi_{T,1,1}^\pm \\ -\phi_{T,1,1}^\pm \\ \phi_{T,1,0}^\pm \\ 0 \end{pmatrix}. \quad (5.8)$$

Here, the normalization factor

$$N_{\Lambda,\Sigma}^\pm = \sqrt{2} \sqrt{1 + \left(\frac{\epsilon_\Lambda - \epsilon_{1,\pm 1} \pm \sqrt{(\epsilon_\Lambda - \epsilon_{1,\pm 1})^2 + (B\mu_B g_\Sigma)^2}}{B\mu_B g_\Sigma} \right)^2} \quad (5.9)$$

is used, note that the expressions do not apply for $B = 0$.

For L states the ratio of the coefficients of the two bright states is 1 and for the T states the ratio is -1 . This is opposite to reference [5]. One possible reason may be the definition of spins. In this work the spin of the empty state in the valance band is used instead of that of the hole.

By analyzing the values of the coefficients, ϕ , in 3D, seen in Figure 5.1 (generated by using the g-factors of PEA_2PbI_4 see Table 3.1), it is found that Ψ_L^- has the largest dark component and the plus states the largest bright components. In 3D the T components are constant since $\epsilon_{1,0} = \epsilon_{1,\pm 1}$ and are pairwise the same, in 2D the T components are dependent on the magnetic field. The lowest energy is E_L^- since $g_L > g_T$ in PEA_2PbI_4 . All energy degeneracies are broken due to the magnetic shifts, for the energies' dependence on the magnetic field see Figure 5.2, depicting both

the 2D and 3D cases. The energies qualitative dependency on the magnetic field is similar to experimental results [5] but quantitatively seems to be about a factor 6 off in its dependency on the magnetic field — for 360 T the energies are similar to the experimental at 60 T. Note that the 3D case is once more generated using the g-factors of PEA_2PbI_4 . Motivated by the comparison being with results from measurements on PEA_2PbI_4 .

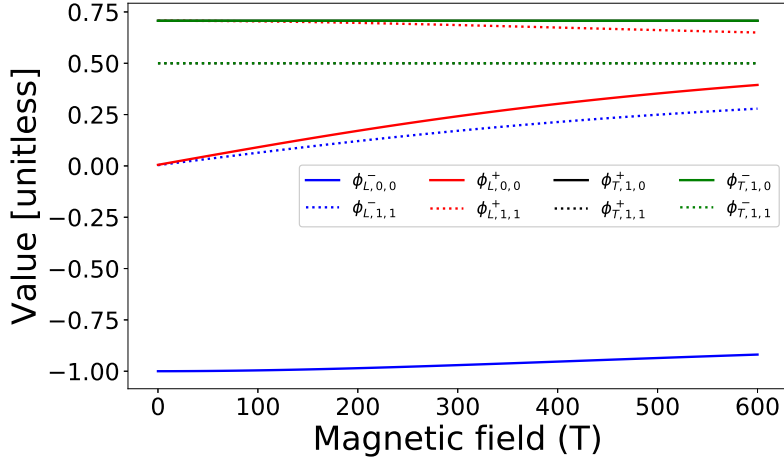
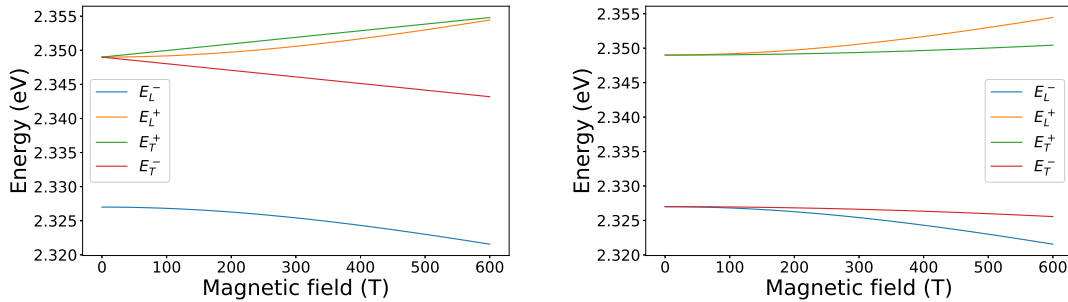


Figure 5.1: Values of coefficients in 3D. Note that Ψ_L^- has the highest absolute valued dark state coefficient. The g-factors of PEA_2PbI_4 have been used since ultimately measurements on that perovskite is the ones compared with. The T^+ and T^- coefficients are overlapping.



(a) The 3D case shows almost the same qualitative dependence as found experimentally for the 2D case, but is quantitatively wrong [5].

(b) The 2D case does not quantitatively neither qualitatively reproduce the experimental results [5]. Falsifying the taken approach for 2D.

Figure 5.2: Energy levels in 2D and 3D. The magnetic field results in four non-degenerate energies. The g-factors of PEA_2PbI_4 have been used in both cases.

Expressing the states in the hybrid basis can be useful when analyzing the spin

configuration of the states

$$\Psi_L^\pm = \frac{1}{N_{(0,0),L}^\pm} \begin{pmatrix} \frac{1}{B\mu_B g_L} (\epsilon_{0,0} - \epsilon_{1,\pm 1} \pm \sqrt{(\epsilon_{0,0} - \epsilon_{1,\pm 1})^2 + (B\mu_B g_L)^2}) \\ 1 \\ 1 \\ \frac{1}{B\mu_B g_L} (\epsilon_{0,0} - \epsilon_{1,\pm 1} \pm \sqrt{(\epsilon_{0,0} - \epsilon_{1,\pm 1})^2 + (B\mu_B g_L)^2}) \end{pmatrix} = \begin{pmatrix} \frac{\phi_{L,0,0}^\pm}{\sqrt{2}} \\ \phi_{L,1,1}^\pm \\ \phi_{L,1,1}^\pm \\ \frac{\phi_{L,0,0}^\pm}{\sqrt{2}} \end{pmatrix} \quad (5.10)$$

and

$$\Psi_T^\pm = \frac{1}{N_{(1,0),T}^\pm} \begin{pmatrix} -\frac{1}{B\mu_B g_T} (\epsilon_{1,0} - \epsilon_{1,\pm 1} \pm \sqrt{(\epsilon_{1,0} - \epsilon_{1,\pm 1})^2 + (B\mu_B g_T)^2}) \\ 1 \\ -1 \\ \frac{1}{B\mu_B g_T} (\epsilon_{1,0} - \epsilon_{1,\pm 1} \pm \sqrt{(\epsilon_{1,0} - \epsilon_{1,\pm 1})^2 + (B\mu_B g_T)^2}) \end{pmatrix} = \begin{pmatrix} \frac{\phi_{T,1,0}^\pm}{\sqrt{2}} \\ \phi_{T,1,1}^\pm \\ -\phi_{T,1,1}^\pm \\ -\frac{\phi_{T,1,0}^\pm}{\sqrt{2}} \end{pmatrix} \quad (5.11)$$

6

Phonon Scattering

Phonon scattering is the most important relaxation process for excitons [3]. In the exciton basis an electron scattering with a phonon is described by Eq. (2.10). Phonon scattering can further be divided into processes which conserve the spin and those which, assisted by a spin flip process, allow for a spin change. A phenomenological spin flipping process will be treated here where a spin flip is allowed but not motivated. For a proper treatment the spin flip process needs to be identified and the expression for the scattering changed accordingly.

6.1 Scattering With Spin Conservation

If spin is considered when transforming Eq. (2.8) to the exciton basis, the following expression expressed in the hybridized exciton basis is obtained

$$\begin{aligned}
H_{ex-ph} &= \sum_{\substack{s,s',s'' \\ \mathbf{q},\mathbf{k},\mathbf{Q} \\ j,n,n'}} \delta_{s,s'} (g_{\mathbf{q}}^{j,c} \phi_{\mathbf{k}+\alpha_n\mathbf{q}}^{1s} \phi_{\mathbf{k}}^{1s*} \theta_{n,\mathbf{Q}+\mathbf{q}}^{ss''} \theta_{n',\mathbf{Q}}^{s's''*}) \\
&\quad - g_{\mathbf{q}}^{j,v} \phi_{\mathbf{k}-\alpha_e\mathbf{q}}^{1s} \phi_{\mathbf{k}}^{\mu*} \theta_{n,\mathbf{Q}+\mathbf{q}}^{s''s'} \theta_{n',\mathbf{Q}}^{s''s'*}) Y_{n,\mathbf{Q}+\mathbf{q}}^\dagger Y_{n',\mathbf{Q}} b_{\mathbf{q}}^j + \\
&\quad + \delta_{s,s'} (g_{\mathbf{q}}^{j,c} \phi_{\mathbf{k}}^{1s} \phi_{\mathbf{k}+\alpha_n\mathbf{q}}^{1s*} \theta_{n,\mathbf{Q}}^{ss''} \theta_{n',\mathbf{Q}+\mathbf{q}}^{s's''*} - g_{\mathbf{q}}^{j,v} \phi_{\mathbf{k}}^{1s} \phi_{\mathbf{k}-\alpha_e\mathbf{q}}^{1s*} \theta_{n,\mathbf{Q}}^{s''s'} \theta_{n',\mathbf{Q}+\mathbf{q}}^{s''s'*}) Y_{n,\mathbf{Q}}^\dagger Y_{n',\mathbf{Q}+\mathbf{q}} b_{\mathbf{q}}^{j\dagger} \\
&= \sum_{s,s'} \theta_n^{ss'} \theta_{n'}^{ss'*} G_{\mathbf{q}}^{j*} Y_{n,\mathbf{Q}+\mathbf{q}}^\dagger Y_{n',\mathbf{Q}} b_{\mathbf{q}}^j + \theta_n^{ss'} \theta_{n'}^{ss'*} G_{\mathbf{q}}^j Y_{n,\mathbf{Q}}^\dagger Y_{n',\mathbf{Q}+\mathbf{q}} b_{\mathbf{q}}^{j\dagger} \\
&= D^{nn'} G_{\mathbf{q}}^{nn'j} Y_{n,\mathbf{Q}}^\dagger Y_{n',\mathbf{Q}+\mathbf{q}} b_{\mathbf{q}}^{j\dagger} + H.C..
\end{aligned} \tag{6.1}$$

The δ -functions are introduced to enforce spin conservation and the element $D^{nn'} = \sum_{s,s'} \theta_n^{ss'} \theta_{n'}^{ss'*}$ to simplify notation. Further note that for the cases considered, that θ is known to be independent of momentum and that only $\mu = \nu = 1s$ states are considered. Then, as in section 2.2 the scattering rate is found to be

$$\Gamma_{\mathbf{Q}}^n = \pi |D^{nn'}|^2 \sum_{j,\mathbf{q},\pm,n'} |G_{\mathbf{q}}^{nn'j}|^2 \left(n_{\mathbf{q}}^j + \frac{1}{2} \pm \frac{1}{2} \right) \delta(E_{\mathbf{k}+\mathbf{q}}^{n'} - E_{\mathbf{k}}^n \pm \hbar\Omega_{\mathbf{q}}^j). \tag{6.2}$$

When studying specific transitions $D^{nn'}$ is crucial and is given by $D^{nn'} = \delta_{n,n'}$, only allowing for scattering between the same states. This is expected since the states are orthogonal to each other (they are independent states) and no spin change is allowed which could break the orthogonality.

6.2 Scattering Without Spin Conservation

In this section spin flip is going to be allowed. This is naively done by simply allowing for a spin change. To investigate this mechanism properly a specific spin flip process needs to be considered, which may change the character of the scattering, and the results here are therefore only indicative. When allowing for spin change the δ -functions are removed from Eq. (6.1). By introducing the scattering element

$$L_{jq}^{nn'} = \sum_{s,s',s''} (g_q^{j,c} F(\alpha_h \mathbf{q}) \theta_n^{ss''} - g_q^{j,v} F(-\alpha_e \mathbf{q}) \theta_n^{s's}) \theta_{n'}^{s's''*} \quad (6.3)$$

with

$$F(\mathbf{x}) = \sum_{\bar{\mathbf{k}}} \phi_{\bar{\mathbf{k}}}^{1s} \phi_{\bar{\mathbf{k}}+\mathbf{x}}^{1s*} \quad (6.4)$$

it is possible to rewrite Eq. (6.1) as (note no δ -functions and that $\theta = \theta^*$)

$$H_{ex-ph} = \sum_{\substack{\mathbf{q}, \mathbf{Q} \\ j, n, n'}} L_{jq}^{nn'*} Y_{n, \mathbf{Q}+\mathbf{q}}^\dagger Y_{n', \mathbf{Q}} b_{\mathbf{q}}^j + L_{jq}^{nn'} Y_{n, \mathbf{Q}}^\dagger Y_{n', \mathbf{Q}+\mathbf{q}} b_{\mathbf{q}}^{j\dagger}, \quad (6.5)$$

with scattering rate

$$\Gamma_{\mathbf{Q}}^n = \pi \sum_{j, \mathbf{q}, \pm, n'} |L_{jq}^{nn'}|^2 \left(n_{\mathbf{q}}^j + \frac{1}{2} \pm \frac{1}{2} \right) \delta(E_{\mathbf{k}+\mathbf{q}}^{n'} - E_{\mathbf{k}}^n \pm \hbar \Omega_{\mathbf{q}}^j). \quad (6.6)$$

To determine the scattering rate $L_{jq}^{nn'}$ needs to be evaluated. By summing over the spins it is found that the relation Eq. (6.3) may quite simply be expressed as $L_{jq}^{nn'} = C^{nn'} G_{\mathbf{q}}^{1s1sj}$. The constants $C^{nn'}$ for the different transitions, with no magnetic field considered, are presented in Table 6.1. It can be seen that scattering between the dark and bright states is now possible.

Transition	$ C^{nn'} $
$\Psi_n \iff \Psi_n$	1
$\Psi_{1, \pm 1}^{\text{bright}} \iff \Psi_{0,0}^{\text{dark}}$ $\Psi_{1, \pm 1}^{\text{bright}} \iff \Psi_{1,0}^{\text{gray}}$	$\frac{1}{\sqrt{2}}$
$\Psi_{1,1}^{\text{bright}} \rightarrow \Psi_{1,1}^{\text{bright}}$ $\Psi_{1,-1}^{\text{bright}} \rightarrow \Psi_{1,-1}^{\text{bright}}$	1
$\Psi_{1,1}^{\text{bright}} \iff \Psi_{1,-1}^{\text{bright}}$ $\Psi_{1,0}^{\text{dark/gray}} \iff \Psi_{0,0}^{\text{dark}}$	0

Table 6.1: Values of the transition constant C between $1s$ states with no magnetic field but with spin flip allowed.

7

Discussion

The qualitative spectrum in 3D is correct and the quantitative results are in the right order of magnitude. In 2D the energy splitting of 25 meV is in agreement with experiments [5] but not the qualitative spectrum, instead of one gray and one dark state the model predicts two dark. The problems are most likely due to a too approximative treatment of the 2D confinement. The phonon scattering results indicate no one-electron scattering with conserved spin, which suggests inefficient scattering since spin changing processes are usually (much) less likely. Such a process would not contradict the experimental results [5]. It would, however, be interesting to further understand these more complex processes. In the following are the model of the exciton spectrum and possible ways of treating the 2D case more accurately discussed. Also the scattering results are addressed and two suggestions for spin changing scattering processes are presented.

Exciton landscape with and without magnetic field

In the 3D case the predicted spectrum is qualitatively correct with two bright, one gray and one dark state as expected [2, 5]. The quantitative result is more difficult to assess since results available in the literature are inconclusive and estimates of the splitting vary [2, 21]. Noting that especially the reliability of the Taylor expansion $e^{i\mathbf{G}\cdot\mathbf{r}} \approx 1 + i\mathbf{G}\cdot\mathbf{r}$ is somewhat questionable, the numerical results of the model are not expected to be accurate. Apart from the factor six in the magnetic field dependence, the energy levels in the magnetic field follow rather well the experimentally measured ones for 2D see Figure 5.2. Another difference is that E_L^- is found to have a slightly higher energy in experiments [5]. This could possibly be corrected by not approximating the perovskite as cubic but using its true symmetry. Note that the g -factors of PEA_2PbI_4 were used in 3D which is of course not correct, but should still be sufficient for the present treatment of the magnetic field.

The treatment of the 2D case, using a δ -confinement function, is most certainly inaccurate. Both the lack of gray states, which are impossible to get when neglecting z components and the degeneracy of the lowest energy level are clear indications of that. It is also evident that completely omitting the components in the out-of-plane direction is an approximation, and apparently that approximation is too coarse to apply in 2D perovskites. At the same time the energy split of 25 meV is reasonable compared with experiments [5] and the good predictions of the 3D model, indicate that a smaller perturbative modification to correctly treat the 2D case could be successful.

An obvious improvement could be to choose a more realistic envelope function than a δ -function. Another envelope function would lead to $\langle S|\hat{\mathbf{p}}f(z)|Z\rangle$ not necessarily

being zero, thus allowing for gray states. Another major problem is that, for the mixing of states and energy splitting of the two lowest states, $\mathbf{A} \cdot \langle S | \hat{\mathbf{p}} | Z \rangle$ needs to be non-zero and not negligible, for receiving a splitting of the gray state comparable to the bright one. Since $\langle S | \hat{\mathbf{p}} | Z \rangle \propto \hat{z}$ it means that a momentum transfer in the z -direction is required. In addition, the envelope function must also be physically reasonable fulfilling the boundary conditions on wavefunctions. Finally, not as fundamental, but important for the applicability, the expression including the envelope function should be possible to evaluate.

Intuitive envelope functions to choose are the wavefunctions of a particle in a quantum well. For a single quantum well there is no periodicity in the z -direction and therefore no G_z , so no short-range part. The problem with the long-range part is that for an infinite quantum well the smallest possible momentum is large, a multiple of $\frac{\pi}{L_{\text{width}}}$, which is outside of the first Brillouin zone, which makes the assumption $\mathbf{q} = \mathbf{G} + \mathbf{q}'$ with \mathbf{q}' small questionable. Another problem may be the discreteness of the allowed momenta.

If instead assuming a finite quantum well the momentum spacing would decrease, maybe enough for giving a small enough smallest momentum and an effectively continuous spectrum. However, for evaluating the momenta, the effective mass in the confined direction is required. This effective mass is within the model infinity, due to the lack of electronic band dispersion in the z -direction. With a valid method of estimating the effective mass the finite quantum well could be a good approach. One problem though, is that the long-range splitting should remain dependent on \mathbf{q} and vanish around $\mathbf{q} \approx 0$.

If instead aiming at the short-range part, periodicity needs to be included in the z -direction to give rise to a G_z component. The material is known to consist of regularly spaced layers, so there is obviously a periodicity. A simple way to enforce this is to choose a periodic envelope function

$$\zeta(z + nR_z) = \begin{cases} 0, & z \in [-\frac{L}{2} + nR_z, -\frac{d}{2} + nR_z] \\ f_{k_z}(z), & z \in [-\frac{d}{2} + nR_z, \frac{d}{2} + nR_z] \\ 0, & z \in [\frac{d}{2} + nR_z, \frac{L}{2} + nR_z] \end{cases}.$$

The problem with this envelope function is that no conditions are put on the momentum in the z -direction (for example \mathbf{k}_{1z} and \mathbf{k}_{4z}) due to the plane waves of the Bloch functions only being in the plane ($e^{i\mathbf{k}_{\parallel} \cdot \mathbf{r}_{\parallel}}$), compare also with Eq. (4.10) where the plane waves give rise to conditions on \mathbf{k}_z . The lack of conditions on \mathbf{k}_z makes the evaluation of $\langle u_{c_{\mathbf{k}_{1z} + \mathbf{q}'_{\parallel} + \mathbf{k}_{4z}}, s_1} | f_{k_{1z}}(z) f_{k_{4z}}(z) e^{i\mathbf{G} \cdot \mathbf{r}} | u_{v_{\mathbf{k}_4}, s_4} \rangle$ tricky. Also, without any value for \mathbf{k}_z the envelope functions for a quantum well

$$f_{k_z}(z) = \begin{cases} \sin k_z z \\ \cos k_z z \end{cases}$$

cannot be evaluated. The problems basically boil down to the same as for a single well — \mathbf{k} cannot be evaluated or cannot be assumed to be small. It is also not certain that an envelope function of that form is valid.

A fundamentally different approach is to include the 2D character of the system through the potential. This should work well as long as the potential remains 3D

and is possible to Fourier transform in a way similar to Eq. (4.5). Finding such a potential and transforming it has, however, proven difficult. The first approach was to assume uniformly distributed charges in the z -direction. This, however, gives a potential that is independent of z -component [22]. Likewise, no solution for two point charges not assuming cylindrical symmetry removing the z -dependence have been found. A third anisotropic Coulomb interaction $A/\sqrt{\frac{|\rho-\rho'|^2}{\gamma^2} + \gamma^2|z-z'|^2}$ has been studied. But has not been possible to Fourier transform in any way giving useful results. There should, however, not be any fundamental problems with the two latter potentials and it may be possible to find ways of using them.

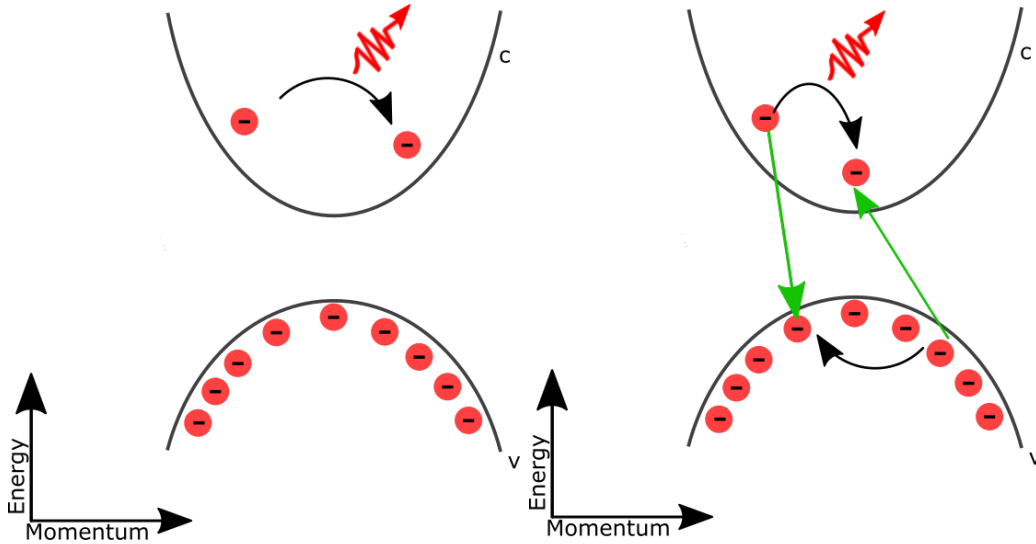
In the preceding, the explored approaches to treat the 2D confinement and the reasons for why they have eventually been abandoned were described. Some of them could, however, be further explored and, given more work, be successful. Other possible approaches could be to go back to a more fundamental level and try to better model the electronic wavefunctions in perovskites and for example extract the effective mass in the z -direction. In this context, reference [23] could be of interest. Another approach could be to try to modify the model of Pikus and Bir to become 2D [24].

Two electron phonon scattering As discussed in chapter 6, assuming spin conservation there cannot be any phonon scattering between different states. This is possible to understand considering that the exciton states are orthogonal - lacking any wave function overlap. All four states considered in this work are having the same spatial wave function (1s) since those have the lowest energy, so the orthogonality uniquely lies with the spin composition, a composition in this work independent of momentum. That is different from when the orthogonality lies in the spatial wave function, then the orthogonality is potentially broken when a momentum transfer \mathbf{q} is accounted for $\sum_{\mathbf{q}} \phi_{\mathbf{k}}^n \phi_{\mathbf{k}+\mathbf{q}}^{n'*}$. Making scattering between for example 2p and 1s states possible. For the same to be possible here, some sort of spin altering process is required.

The required spin change could for example come from chiral phonons. Such phonons may be able to change the spin when interacting, possible by the interaction $\lambda_{\mathbf{k}+\mathbf{q},s}^\dagger \lambda_{\mathbf{k},s'} b_{\mathbf{q},s-s'}$. From section 6.2 such a process is indicated to enable scattering from bright to dark states. However, these interactions and character of the phonons need to be further understood before any conclusions can be drawn. Crucial is the character of the interaction, is the angular momentum of the chiral phonon really able to change the spin and in that case how precisely do the angular momentum of the phonon have to match that of a spin flip $s - s'$. Perhaps it is rather the conservation of angular momentum that should be considered. A part of further understanding this is of course to investigate what chiral phonons, if any, that are present in the studied perovskites and what total angular momentum they are carrying.

Another possibility, exploring the spin mix of the perovskites, is by considering two electron scattering. In the interaction defined in equation (2.8) one electron is changing its momentum upon phonon scattering staying in the same band, see Figure 7.1a. Staying in the same band the spin is well defined and cannot change. On the other hand, a four electron operator process $\lambda_{\mathbf{k}_1,s_1}^\dagger \lambda_{\mathbf{k}_4,s_4} \lambda_{\mathbf{k}_2,s_2}^\dagger \lambda_{\mathbf{k}_3,s_3}'$ ($\lambda \neq \lambda'$) as seen in Figure 7.1b could take place both within the same (black arrows) and

between bands (green arrows), compare with the electron-hole exchange interaction. In this case there could actually be a spin change since a spin in the conduction band has an overlap with both up and down spin in the valance band see Equation (3.1). Since the exchange interaction needs to be considered for getting the accurate states in perovskites, it is not far-fetched that so should also be the case for the scattering. Future studies of the origin of scattering in perovskites seem very interesting.



(a) An electron interacting with a phonon. (b) Two electrons interacting with a phonon.

Figure 7.1: The figures shows the band structure around the gamma point for conduction and valance band under parabolic approximation. Momentum on the x -axis and energy on the y -axis. Electrons are denoted by red circles and phonons with a red arrow. Black arrows indicates momentum change of electrons within bands and green the equivalent exchange process. The latter allowing for a spin change.

Bibliography

- [1] Q. A. Akkerman and L. Manna, “What Defines a Halide Perovskite?” *ACS Energy Letters*, vol. 5, no. 2, pp. 604–610, 2020.
- [2] M. A. Becker, R. Vaxenburg, G. Nedelcu, P. C. Sercel, A. Shabaev, M. J. Mehl, J. G. Michopoulos, S. G. Lambrakos, N. Bernstein, J. L. Lyons, T. Stöferle, R. F. Mahrt, M. V. Kovalenko, D. J. Norris, G. Rainò, and A. L. Efros, “Bright triplet excitons in caesium lead halide perovskites,” *Nature*, vol. 553, pp. 189–193, 2018.
- [3] D. Feldstein, R. Perea-Causín, S. Wang, M. Dyksik, K. Watanabe, T. Taniguchi, P. Plochocka, and E. Malic, “Microscopic Picture of Electron–Phonon Interaction in Two-Dimensional Halide Perovskites,” *The Journal of Physical Chemistry Letters*, vol. 11, no. 23, pp. 9975–9982, 2020. [Online]. Available: <https://doi.org/10.1021/acs.jpcllett.0c02661>
- [4] D. Marongiu, M. Saba, F. Quochi, A. Mura, and G. Bongiovanni, “The role of excitons in 3D and 2D lead halide perovskites,” *J. Mater. Chem. C*, vol. 7, pp. 12 006–12 018, 2019.
- [5] M. Dyksik, H. Duim, D. K. Maude, M. Baranowski, M. A. Loi, and P. Plochocka, “Brightening of dark excitons in 2D perovskites,” *Science advances*, vol. 7, no. 46, p. eabk0904, 2021.
- [6] F. Katsch, M. Selig, A. Carmele, and A. Knorr, “Theory of exciton–exciton interactions in monolayer transition metal dichalcogenides,” *physica status solidi (b)*, vol. 255, no. 12, p. 1800185, 2018. [Online]. Available: <https://onlinelibrary.wiley.com/doi/abs/10.1002/pssb.201800185>
- [7] D. Erkensten, S. Brem, K. Wagner, R. Gillen, R. Perea-Causín, J. D. Ziegler, T. Taniguchi, K. Watanabe, J. Maultzsch, A. Chernikov *et al.*, “Dark exciton–exciton annihilation in monolayer wse 2,” *Physical Review B*, vol. 104, no. 24, p. L241406, 2021.
- [8] R. Rosati, R. Schmidt, S. Brem, R. Perea-Causín, I. Niehues, J. Kern, J. A. Preuß, R. Schneider, S. Michaelis de Vasconcellos, R. Bratschitsch *et al.*, “Dark exciton anti-funneling in atomically thin semiconductors,” *Nature Communications*, vol. 12, no. 1, pp. 1–7, 2021.
- [9] E. Malic, J. Maultzsch, S. Reich, and A. Knorr, “Excitonic rayleigh scattering spectra of metallic single-walled carbon nanotubes,” *Physical Review B*, vol. 82, no. 11, p. 115439, 2010.

- [10] G. Berghäuser, P. Steinleitner, P. Merkl, R. Huber, A. Knorr, and E. Malic, “Mapping of the dark exciton landscape in transition metal dichalcogenides,” *Physical Review B*, vol. 98, no. 2, p. 020301, 2018.
- [11] P. Hofmann, *Solid State Physics*. Wiley-VCH Verlag GmbH, 2015.
- [12] G. D. Mahan, *Many-particle physics*. Springer Science & Business Media, 2013.
- [13] S. Brem, J. Zipfel, M. Selig, A. Raja, L. Waldecker, J. D. Ziegler, T. Taniguchi, K. Watanabe, A. Chernikov, and E. Malic, “Intrinsic lifetime of higher excitonic states in tungsten diselenide monolayers,” *Nanoscale*, vol. 11, no. 25, pp. 12 381–12 387, 2019.
- [14] M. Feierabend, *Microscopic Theory of Externally Tunable Exciton Signatures of Two-Dimensional Materials*. Chalmers Tekniska Hogskola (Sweden), 2021.
- [15] M. Feierabend, S. Brem, A. Ekman, and E. Malic, “Brightening of spin-and momentum-dark excitons in transition metal dichalcogenides,” *2D Materials*, vol. 8, p. 015013, 2020.
- [16] R. Ben Aich, I. Saïdi, S. Ben Radhia, K. Boujdaria, T. Barisien, L. Legrand, F. Bernardot, M. Chamarro, and C. Testelin, “Bright-exciton splittings in inorganic cesium lead halide perovskite nanocrystals,” *Phys. Rev. Applied*, vol. 11, p. 034042, Mar 2019. [Online]. Available: <https://link.aps.org/doi/10.1103/PhysRevApplied.11.034042>
- [17] J. M. Urban, G. Chehade, M. Dyksik, M. Menahem, A. Surrente, G. Trippé-Allard, D. K. Maude, D. Garrot, O. Yaffe, E. Deleporte, P. Plochocka, and M. Baranowski, “Revealing excitonic phonon coupling in $(\text{PEA})_2(\text{MA})_{n-1}\text{Pb}_n\text{I}_{3n+1}$ 2D layered perovskites,” *The Journal of Physical Chemistry Letters*, vol. 11, no. 15, pp. 5830–5835, 2020.
- [18] J. D. Ziegler, J. Zipfel, B. Meisinger, M. Menahem, X. Zhu, T. Taniguchi, K. Watanabe, O. Yaffe, D. A. Egger, and A. Chernikov, “Fast and anomalous exciton diffusion in two-dimensional hybrid perovskites,” *Nano Letters*, vol. 20, no. 9, pp. 6674–6681, 2020.
- [19] H. Haug and S. W. Koch, *Quantum Theory of the Optical and Electronic Properties of Semiconductors*. World Scientific, 2009.
- [20] L. Pengke, R. Cedric, V. T. Dinh, R. Lei, M. Xavier, and D. Hanan, “Intervalley electron-hole exchange interaction and impurity-assisted recombination of indirect excitons in WS_2 and WSe_2 monolayers,” *arXiv preprint arXiv:2205.00090*, 2022.
- [21] K. Xu, J. F. Vliem, and A. Meijerink, “Long-lived dark exciton emission in Mn-doped CsPbCl_3 perovskite nanocrystals,” *The Journal of Physical Chemistry C*, pp. 979–984, 2018.
- [22] S. Latini, T. Olsen, and K. S. Thygesen, “Excitons in van der Waals heterostructures: The important role of dielectric screening,” *Physical Review B*, vol. 92, no. 24, p. 245123, 2015.

- [23] Z. G. Yu, “Effective-mass model and magneto-optical properties in hybrid perovskites,” *Scientific Reports*, vol. 6, no. 1, pp. 1–14, 2016.
- [24] G. L. Bir and G. E. Pikus, *Symmetry and Strain Induced Effects in Semiconductors*. Wiley, 1975.

A

Perturbation

For evaluating the overlaps in Eq. (4.9) and terms of the form $d_{ss'}^{\lambda\lambda'} = \langle \lambda s | \hat{p} | \lambda' s' \rangle$ in Eq. (4.12), perturbation theory may be used. In perturbation theory a disturbance is added to the ground state Hamiltonian (denoted by 0) which results in changes of the wavefunctions Ψ_n and energies E_{nk} . The following notation is used (note that the notation is different from in the rest of the thesis and that any discrepancy should be considered an error in the appendix)

$$\begin{aligned}
 H &= H_0 + \lambda H' \\
 \Psi_{n,\mathbf{k}+q,s} &= \Psi_{nks}^0 + \lambda \Psi'_{nks} + \lambda^2 \Psi''_{nks}, \quad |n, \mathbf{k} + \mathbf{q}, s\rangle = |n\mathbf{k}s\rangle^0 + \lambda |n\mathbf{k}s\rangle' + \lambda^2 |n\mathbf{k}s\rangle'' \\
 E_{nk} &= E_{nk}^0 + \lambda E'_{nk} + \lambda^2 E''_{nk}
 \end{aligned} \tag{A.1}$$

The Schrödinger equation is

$$H \Psi_{n,\mathbf{k}+q,s} = E_{nk} \Psi_{nks}$$

which can be expanded according to

$$\begin{aligned}
 &(H_0 + \lambda H')(|n\mathbf{k}s\rangle^0 + \lambda |n\mathbf{k}s\rangle' + \lambda^2 |n\mathbf{k}s\rangle'') \\
 &= (E_{nk}^0 + \lambda E'_{nk} + \lambda^2 E''_{nk})(|n\mathbf{k}s\rangle^0 + \lambda |n\mathbf{k}s\rangle' + \lambda^2 |n\mathbf{k}s\rangle'').
 \end{aligned} \tag{A.2}$$

The expression in Eq. (A.2) can be grouped after order in λ

$$\begin{aligned}
 \lambda^0 : & \quad H_0 |n\mathbf{k}s\rangle^0 = E_{nk}^0 |n\mathbf{k}s\rangle^0 \\
 \lambda^1 : & \quad H_0 |n\mathbf{k}s\rangle' + H' |n\mathbf{k}s\rangle^0 = E_{nk}^0 |n\mathbf{k}s\rangle' + E'_{nk} |n\mathbf{k}s\rangle^0 \\
 \lambda^2 : & \quad H_0 |n\mathbf{k}s\rangle'' + H' |n\mathbf{k}s\rangle' = E_{nk}^0 |n\mathbf{k}s\rangle'' + E'_{nk} |n\mathbf{k}s\rangle' + E''_{nk} |n\mathbf{k}s\rangle^0
 \end{aligned}$$

and by further multiplying λ^1 by $\langle n\mathbf{k}s|^0$ Eq. (A.3) is obtained

$$\begin{aligned}
 \langle n\mathbf{k}s|^0 H_0 |n\mathbf{k}s\rangle' + \langle n\mathbf{k}s|^0 H' |n\mathbf{k}s\rangle^0 &= \langle n\mathbf{k}s|^0 E_{nk}^0 |n\mathbf{k}s\rangle' + \langle n\mathbf{k}s|^0 E'_{nk} |n\mathbf{k}s\rangle^0 \\
 \longrightarrow \langle n\mathbf{k}s|^0 H' |n\mathbf{k}s\rangle^0 &= E'_{nk}.
 \end{aligned} \tag{A.3}$$

Further it is noted that

$$H' |n\mathbf{k}s\rangle^0 = \sum_{\substack{\text{if } n' \neq n, s' \\ \text{else } s' \neq s}} |n'\mathbf{k}s'\rangle^0 \langle n'\mathbf{k}s'|^0 H' |n\mathbf{k}s\rangle^0 + |n\mathbf{k}s\rangle^0 \langle n\mathbf{k}s|^0 H' |n\mathbf{k}s\rangle^0 \quad (\text{A.4})$$

which is used for the λ^1 -expression giving

$$\begin{aligned} H_0 |n\mathbf{k}s\rangle' + \sum_{\substack{\text{if } n' \neq n, s' \\ \text{else } s' \neq s}} |n'\mathbf{k}s'\rangle^0 \langle n'\mathbf{k}s'|^0 H' |n\mathbf{k}s\rangle^0 + |n\mathbf{k}s\rangle^0 \langle n\mathbf{k}s|^0 H' |n\mathbf{k}s\rangle^0 \\ = E_{n\mathbf{k}}^0 |n\mathbf{k}s\rangle' + E'_{n\mathbf{k}} |n\mathbf{k}s\rangle^0 \quad . \quad (\text{A.5}) \\ \longrightarrow H_0 |n\mathbf{k}s\rangle' + \sum_{\substack{\text{if } n' \neq n, s' \\ \text{else } s' \neq s}} |n'\mathbf{k}s'\rangle^0 \langle n'\mathbf{k}s'|^0 H' |n\mathbf{k}s\rangle^0 = E_{n\mathbf{k}}^0 |n\mathbf{k}s\rangle' \end{aligned}$$

By first multiplying by $\langle n''\mathbf{k}s''|^0$

$$\begin{aligned} \langle n''\mathbf{k}s''|^0 H_0 |n\mathbf{k}s\rangle' + \sum_{\substack{\text{if } n' \neq n, s' \\ \text{else } s' \neq s}} \underbrace{\langle n''\mathbf{k}s''|^0 |n'\mathbf{k}s'\rangle^0}_{\delta_{n'',n'} \delta_{s'',s'}} \langle n'\mathbf{k}s'|^0 H' |n\mathbf{k}s\rangle^0 = \langle n''\mathbf{k}s''|^0 E_{n\mathbf{k}}^0 |n\mathbf{k}s\rangle' \\ \longrightarrow \sum_{\substack{\text{if } n'' \neq n, s'' \\ \text{else } s'' \neq s}} \langle n''\mathbf{k}s''|^0 H' |n\mathbf{k}s\rangle^0 = (E_{n\mathbf{k}}^0 - E_{n''\mathbf{k}}^0) \langle n''\mathbf{k}s''|^0 |n\mathbf{k}s\rangle' \end{aligned} \quad (\text{A.6})$$

and then by $|n''\mathbf{k}s''\rangle^0$, the following expression is obtained

$$\begin{aligned} |n\mathbf{k}s\rangle' &= \sum_{\substack{\text{if } n'' \neq n, s'' \\ \text{else } s'' \neq s}} \frac{\langle n''\mathbf{k}s''|^0 H' |n\mathbf{k}s\rangle^0}{E_{n\mathbf{k}}^0 - E_{n''\mathbf{k}}^0} |n''\mathbf{k}s''\rangle^0 \\ &= \frac{\hbar\mathbf{q}}{m} \sum_{\substack{\text{if } n'' \neq n, s'' \\ \text{else } s'' \neq s}} \frac{\langle n''\mathbf{k}s''|^0 \hat{p} |n\mathbf{k}s\rangle^0}{E_{n\mathbf{k}}^0 - E_{n''\mathbf{k}}^0} |n''\mathbf{k}s''\rangle^0 . \end{aligned} \quad (\text{A.7})$$

To the first order the perturbed bloch functions are then given by

$$|n, \mathbf{k} + \mathbf{q}, s\rangle = |n\mathbf{k}s\rangle^0 + \frac{\hbar\mathbf{q}}{m} \sum_{\substack{\text{if } n'' \neq n, s'' \\ \text{else } s'' \neq s}} \frac{\langle n''\mathbf{k}s''|^0 \hat{p} |n\mathbf{k}s\rangle^0}{E_{n\mathbf{k}}^0 - E_{n''\mathbf{k}}^0} |n''\mathbf{k}s''\rangle^0, \quad (\text{A.8})$$

which can be used for getting the first factor in Eq. (4.9), namely

$$\begin{aligned}
& \langle u_{c\mathbf{k}_4+q,s_1} | u_{v\mathbf{k}_4,s_4} \rangle = \langle u_{c\mathbf{k}_4,s_1} | u_{v\mathbf{k}_4,s_4} \rangle \\
& + \frac{\hbar\mathbf{q}}{m} \sum_{\substack{\text{if } n'' \neq c, s'' \\ \text{else } s'' \neq s_1}} \left(\frac{\langle n''\mathbf{k}_4 s'' |^0 \hat{p} | c\mathbf{k}_4 s_1 \rangle^0}{E_{c\mathbf{k}_4}^0 - E_{n''\mathbf{k}_4}^0} \right)^* * \langle n''\mathbf{k}_4 s'' |^0 u_{v\mathbf{k}_4,s_4} \rangle \\
& = \frac{\hbar\mathbf{q}}{m} \sum_{s''} \left(\frac{\langle v\mathbf{k}_4 s'' |^0 \hat{p} | c\mathbf{k}_4 s_1 \rangle^0}{E_{c\mathbf{k}_4}^0 - E_{v\mathbf{k}_4}^0} \right)^* * \delta_{s'',s_4} \\
& + \frac{\hbar\mathbf{q}}{m} \sum_{s_4 \neq s_1} \left(\frac{\langle c\mathbf{k}_4 s_4 |^0 \hat{p} | c\mathbf{k}_4 s_1 \rangle^0}{E_{c\mathbf{k}_4}^0 - E_{c\mathbf{k}_4}^0} \right)^* * \langle c\mathbf{k}_4 s'' |^0 u_{v\mathbf{k}_4,s_4} \rangle \\
& = \frac{\hbar\mathbf{q}}{m} \left(\frac{\langle v\mathbf{k}_4 s_4 |^0 \hat{p} | c\mathbf{k}_4 s_1 \rangle^0}{E_{c\mathbf{k}_4}^0 - E_{v\mathbf{k}_4}^0} \right)^* * = \frac{\hbar\mathbf{q}}{m} \frac{\langle c\mathbf{k}_4 s_1 |^0 \hat{p} | v\mathbf{k}_4 s_4 \rangle^0}{E_{c\mathbf{k}_4}^0 - E_{v\mathbf{k}_4}^0} = \frac{\hbar}{mE_g} \mathbf{q} \cdot d_{s_1 s_4}^{cv}.
\end{aligned} \tag{A.9}$$

Assuming the momentum operator does not change spin the second term in the second line is zero, and the division by 0 is not a problem. The other factor in Eq. (4.9) is in the same way found to be

$$\begin{aligned}
& \langle u_{v\mathbf{k}_3-q,s_2} | u_{c\mathbf{k}_3,s_3} \rangle = \langle u_{v\mathbf{k}_3,s_2} | u_{c\mathbf{k}_3,s_3} \rangle \\
& - \frac{\hbar\mathbf{q}}{m} \sum_{\substack{\text{if } n'' \neq v, s'' \\ \text{else } s'' \neq s_2}} \left(\frac{\langle n''\mathbf{k}_3 s'' |^0 \hat{p} | v\mathbf{k}_3 s_2 \rangle^0}{E_{v\mathbf{k}_3}^0 - E_{n''\mathbf{k}_3}^0} \right)^* * \langle n''\mathbf{k}_3 s'' |^0 u_{c\mathbf{k}_3,s_3} \rangle \\
& = - \frac{\hbar\mathbf{q}}{m} \left(\frac{\langle c\mathbf{k}_3 s_3 |^0 \hat{p} | v\mathbf{k}_3 s_2 \rangle^0}{E_{v\mathbf{k}_3}^0 - E_{c\mathbf{k}_3}^0} \right)^* * = - \frac{\hbar\mathbf{q}}{m} \frac{\langle v\mathbf{k}_3 s_2 |^0 \hat{p} | c\mathbf{k}_3 s_3 \rangle^0}{E_{v\mathbf{k}_3}^0 - E_{c\mathbf{k}_3}^0} = \frac{\hbar}{mE_g} \mathbf{q} \cdot d_{s_3 s_2}^{cv*}.
\end{aligned} \tag{A.10}$$

Eq. (4.9) now becomes

$$\sum_{\substack{\mathbf{k}_3, \mathbf{k}_4, \mathbf{q} \\ s_1, s_2, s_3, s_4}} \frac{\hbar}{E_g m} \frac{\hbar}{E_g m} \mathbf{q} \cdot d_{s_3 s_2}^{cv*} \mathbf{q} \cdot d_{s_1 s_4}^{cv} V_{\mathbf{q}}. \tag{A.11}$$

By continuing with perturbation it is possible to evaluate Eq. (A.11), starting by multiplying λ^1 by $\langle n'\mathbf{k}s' |^0$ which gives

$$\begin{aligned}
& \langle n'\mathbf{k}s' |^0 H_0 | n\mathbf{k}s \rangle' + \langle n'\mathbf{k}s' |^0 H' | n\mathbf{k}s \rangle^0 = \langle n'\mathbf{k}s' |^0 E_{n\mathbf{k}}^0 | n\mathbf{k}s \rangle' + \langle n'\mathbf{k}s' |^0 E'_{n\mathbf{k}} | n\mathbf{k}s \rangle^0 \\
& (E_{n'\mathbf{k}}^0 - E_{n\mathbf{k}}^0) \langle n'\mathbf{k}s' |^0 | n\mathbf{k}s \rangle' + \langle n'\mathbf{k}s' |^0 H' | n\mathbf{k}s \rangle^0 = E'_{n\mathbf{k}} \langle n'\mathbf{k}s' |^0 | n\mathbf{k}s \rangle^0.
\end{aligned} \tag{A.12}$$

Then the case $n' = n$, $s' = s$ is considered, yielding

$$\langle n\mathbf{k}s |^0 H' | n\mathbf{k}s \rangle^0 = E'_{n\mathbf{k}} = \frac{\hbar^2 \mathbf{k}^2}{2m}. \tag{A.13}$$

Further is Eq. (A.4) multiplied by $\langle n''\mathbf{k}s'' |^0$ resulting in

$$\begin{aligned}
& \langle n'' \mathbf{k} s'' |^0 H' | n \mathbf{k} s \rangle^0 \\
&= \sum_{\substack{\text{if } n' \neq n, s' \\ \text{else } s' \neq s}} \langle n'' \mathbf{k} s'' |^0 | n' \mathbf{k} s' \rangle^0 \langle n' \mathbf{k} s' |^0 H' | n \mathbf{k} s \rangle^0 + \langle n'' \mathbf{k} s'' |^0 | n \mathbf{k} s \rangle^0 E'_{n\mathbf{k}} \\
&= \sum_{\substack{\text{if } n'' \neq n, s'' \\ \text{else } s'' \neq s}} \langle n'' \mathbf{k} s'' |^0 H' | n \mathbf{k} s \rangle^0 + \langle n'' \mathbf{k} s' |^0 | n \mathbf{k} s \rangle^0 E'_{n\mathbf{k}}
\end{aligned} \tag{A.14}$$

which can be used in Eq. (A.12) resulting in

$$\begin{aligned}
& (E_{n'\mathbf{k}}^0 - E_{n\mathbf{k}}^0) \langle n' \mathbf{k} s' |^0 | n \mathbf{k} s \rangle' + \sum_{\substack{\text{if } n' \neq n, s' \\ \text{else } s' \neq s}} \langle n' \mathbf{k} s' |^0 H' | n \mathbf{k} s \rangle^0 + \langle n' \mathbf{k} s' |^0 | n \mathbf{k} s \rangle^0 E'_{n\mathbf{k}} \\
&= E'_{n\mathbf{k}} \langle n' \mathbf{k} s' |^0 | n \mathbf{k} s \rangle^0, \\
& \langle n' \mathbf{k} s' |^0 | n \mathbf{k} s \rangle' = \sum_{\substack{\text{if } n' \neq n, s' \\ \text{else } s' \neq s}} \frac{\langle n' \mathbf{k} s' |^0 H' | n \mathbf{k} s \rangle^0}{(E_{n\mathbf{k}}^0 - E_{n'\mathbf{k}}^0)} = \sum_{\substack{\text{if } n' \neq n, s' \\ \text{else } s' \neq s}} \frac{\langle n' \mathbf{k} s' |^0 \frac{\hbar \mathbf{k} \hat{p}}{m} | n \mathbf{k} s \rangle^0}{(E_{n\mathbf{k}}^0 - E_{n'\mathbf{k}}^0)}.
\end{aligned} \tag{A.15}$$

Multiplying by $|n' \mathbf{k} s' \rangle^0$ gives

$$|n \mathbf{k} s \rangle' = \sum_{\substack{\text{if } n' \neq n, s' \\ \text{else } s' \neq s}} \frac{\hbar \mathbf{k}}{m} \frac{\langle n' \mathbf{k} s' |^0 \hat{p} | n \mathbf{k} s \rangle^0}{(E_{n\mathbf{k}}^0 - E_{n'\mathbf{k}}^0)} |n' \mathbf{k} s' \rangle^0. \tag{A.16}$$

Then multiplying λ^2 by $\langle n \mathbf{k} s |^0$ gives

$$\begin{aligned}
& E_{n\mathbf{k}}^0 \langle n \mathbf{k} s |^0 | n \mathbf{k} s \rangle'' + \langle n \mathbf{k} s |^0 H' | n \mathbf{k} s \rangle' \\
&= E_{n\mathbf{k}}^0 \langle n \mathbf{k} s |^0 | n \mathbf{k} s \rangle'' + E'_{n\mathbf{k}} \langle n \mathbf{k} s |^0 | n \mathbf{k} s \rangle' + E''_{n\mathbf{k}} \langle n \mathbf{k} s |^0 | n \mathbf{k} s \rangle^0, \\
& \langle n \mathbf{k} s |^0 H' | n \mathbf{k} s \rangle' = E''_{n\mathbf{k}}
\end{aligned} \tag{A.17}$$

Multiplication of Eq. (A.16) with $\langle n \mathbf{k} s |^0 H'$ gives

$$\begin{aligned}
E''_{n\mathbf{k}} &= \langle n \mathbf{k} s |^0 H' \frac{\hbar \mathbf{k}}{m} \sum_{\substack{\text{if } n' \neq n, s' \\ \text{else } s' \neq s}} \frac{\langle n' \mathbf{k} s' |^0 \hat{p} | n \mathbf{k} s \rangle^0}{(E_{n\mathbf{k}}^0 - E_{n'\mathbf{k}}^0)} |n' \mathbf{k} s' \rangle^0 \\
&= \langle n \mathbf{k} s |^0 \frac{\hbar \mathbf{k}}{m} \frac{\hbar \mathbf{k} \hat{p}}{m} \frac{1}{\Delta_{n, \bar{n}}} \sum_{\substack{\text{if } n' \neq n, s' \\ \text{else } s' \neq s}} d_{s', s}^{n', n} |n' \mathbf{k} s' \rangle^0 = \left(\frac{\hbar \mathbf{k} |d_{s, \bar{s}}^{n, \bar{n}}|}{m} \right)^2 \frac{1}{\Delta_{n, \bar{n}}}.
\end{aligned} \tag{A.18}$$

The harmonic approximation can then be used around the band minimum to get an expression for the energy, only considering the x -direction Eq. (A.19) is obtained

$$E_{n\mathbf{k}} = \frac{1}{2}E_g + \frac{\hbar^2\mathbf{k}^2}{2m} + \left(\frac{\hbar\mathbf{k}|d_{s,\bar{s}}^{n,\bar{n}}|}{m}\right)^2 \frac{1}{\Delta_{n,\bar{n}}} = \frac{1}{2}E_g + \frac{\hbar^2\mathbf{k}^2}{2m_n}. \quad (\text{A.19})$$

$$|d_{s,\bar{s}}^{n,\bar{n}}|^2 = \frac{m\Delta_{n,\bar{n}}}{2} \left(\frac{m}{m_n} - 1\right) \quad (\text{A.20})$$

Considering the additional directions as well and summing gives an additional factor c , note $|d_{s,\bar{s}}^{n,\bar{n}}|^2 = |d_{\bar{s},s}^{\bar{n},n}|^2 = |d_{\bar{s},\bar{s}}^{n,\bar{n}}|^2 = |d_{s,s}^{\bar{n},n}|^2 = |d|^2$ and $\Delta_{n,\bar{n}} = -\Delta_{\bar{n},n}$ which is used to get a relation for d

$$\begin{aligned} c|d|^2 &= \frac{c}{2} \left(|d_{s,\bar{s}}^{n,\bar{n}}|^2 + |d_{\bar{s},s}^{\bar{n},n}|^2 \right) = \frac{m\Delta_{n,\bar{n}}}{2} \left(\frac{m}{m_n} - 1 \right) + \frac{m\Delta_{\bar{n},n}}{2} \left(\frac{m}{m_{\bar{n}}} - 1 \right) \\ &= \frac{m\Delta_{n,\bar{n}}}{2} \left(\frac{m}{m_n} - 1 \right) - \frac{m\Delta_{n,\bar{n}}}{2} \left(\frac{m}{m_{\bar{n}}} - 1 \right) = \frac{m\Delta_{n,\bar{n}}}{2} \left(\frac{m}{m_n} - \frac{m}{m_{\bar{n}}} \right) \end{aligned} \quad (\text{A.21})$$

which in turn gives

$$d_{s,s'}^{cv} = \sqrt{\frac{m^2 E_g}{c} \frac{1}{m_\mu}}. \quad (\text{A.22})$$

Note that there is no momentum or spin dependence.

B

Vector Components of Dipole Matrix Elements

The matrix elements $\langle S | \hat{p} | P_i \rangle$ point in the same direction as $\langle S | \nabla | P_i \rangle$. The nabla operator in spherical coordinates is

$$\begin{aligned} \nabla = & (\sin \theta \cos \phi \hat{x} + \sin \theta \sin \phi \hat{y} + \cos \theta \hat{z}) \frac{d}{dr} + \frac{1}{r} (\cos \theta \cos \phi \hat{x} + \cos \theta \sin \phi \hat{y} - \sin \theta \hat{z}) \frac{d}{d\theta} \\ & + \frac{1}{r \sin \theta} (-\sin \phi \hat{x} + \cos \phi \hat{y}) \frac{d}{d\phi}. \end{aligned} \quad (\text{B.1})$$

The S and P orbitals are having the same angular symmetry as the corresponding hydrogenic wavefunctions, mathematically in spherical coordinates the angular dependency may be expressed as

$$\begin{aligned} \Psi_{1s} & \propto C_1, \\ \Psi_{p_z} & \propto \cos \theta, \\ \Psi_{p_x} & \propto \sin \theta \cos \phi, \\ \Psi_{p_y} & \propto \sin \theta \sin \phi. \end{aligned} \quad (\text{B.2})$$

Only considering the angular part of $\langle S | \nabla | P_i \rangle$ and removing all constants factors the overlap is

$$\begin{aligned} \langle S | \nabla | P_x \rangle = & \int \sin \theta \hat{x} \left(\sin \theta \cos \phi \frac{d}{dr} + \frac{1}{r} \cos \theta \cos \phi \frac{d}{d\theta} + \frac{1}{r \sin \theta} (-\sin \phi \frac{d}{d\phi}) \right) \sin \theta \cos \phi \\ & + \sin \theta \hat{y} \left(\sin \theta \sin \phi \frac{d}{dr} + \frac{1}{r} \cos \theta \sin \phi \frac{d}{d\theta} + \frac{1}{r \sin \theta} \cos \phi \frac{d}{d\phi} \right) \sin \theta \cos \phi \\ & + \sin \theta \hat{z} \left(\cos \theta \frac{d}{dr} - \frac{1}{r} \sin \theta \frac{d}{d\theta} \right) \sin \theta \cos \phi d\phi d\theta \\ & \propto \sin \theta \hat{x} \left(\sin \theta \frac{d}{dr} + \frac{1}{r} \cos \theta \frac{d}{d\theta} + \frac{1}{r \sin \theta} \right) \sin \theta d\theta. \end{aligned} \quad (\text{B.3})$$

Terms in the \hat{y} -direction will all contain the factor $\int_0^{2\pi} \sin \phi \cos \phi d\phi$ and therefore vanish same for the \hat{z} -direction and $\int_0^{2\pi} \cos \phi d\phi$. The ϕ integral in \hat{x} is $\int_0^{2\pi} \cos^2 \phi d\phi = \pi$. In the same way it is possible to show $\langle S | \nabla | P_y \rangle = \propto \hat{y}$, $\langle S | \nabla | P_z \rangle = \propto \hat{z}$.

DEPARTMENT OF PHYSICS
CHALMERS UNIVERSITY OF TECHNOLOGY
Gothenburg, Sweden
www.chalmers.se



CHALMERS
UNIVERSITY OF TECHNOLOGY